



Bachelor Thesis

A Framework for Studies of Physiological Control Systems Applied to Ventricular Assist Devices

Roger de Almeida Matos Júnior

Adviser:

Ph.D. Thiago Damasceno Cordeiro

Maceió, Alagoas
January 30, 2023

Roger de Almeida Matos Júnior

A Framework for Studies of Physiological Control Systems Applied to Ventricular Assist Devices

Bachelor Thesis submitted to the Instituto de Computação of the Universidade Federal de Alagoas as a partial requirement to obtain the bachelor's degree in Computer Engineering.

Adviser:

Ph.D. Thiago Damasceno Cordeiro

Maceió, Alagoas
January 30, 2023

Catálogo na fonte
Universidade Federal de Alagoas
Biblioteca Central
Divisão de Tratamento Técnico

Bibliotecária: Helena Cristina Pimentel do Vale CRB4 - 661

M433f Matos Júnior, Roger de Almeida.
A framework for studies of physiological control systems applied to ventricular assist devices / Roger de Almeida Matos Júnior. – 2023.
46 f. [10] : il.

Orientador: Thiago Damasceno Cordeiro.
Monografia (Bacharelado em Engenharia da Computação) – Universidade Federal de Alagoas. Instituto de Computação. Maceió, 2023.

Bibliografia: f. 44-46.

1. Modelo do sistema cardiovascular. 2. Dispositivo de assistência ventricular.
3. Sistemas fisiológicos. 4. Controle starling-like. 5. Engenharia biomédica. I. Título.

CDU: 004.78:61

Bachelor Thesis submitted to the Instituto de Computação of the Universidade Federal de Alagoas as a partial requirement to obtain the bachelor's degree in Computer Engineering, approved by the examining board who sign below.

Ph.D. Thiago Damasceno Cordeiro - Adviser
Instituto de Computação
Universidade Federal de Alagoas

M.Sc. Luís Felipe Vieira Silva - Examiner
Centro Universitário Mario Pontes Jucá

Ph.D. Tiago Alves de Almeida - Examiner
Instituto de Computação
Universidade Federal de Alagoas

Maceió, Alagoas
January 30, 2023

Acknowledgments

I am incredibly grateful to my adviser, professor Ph.D. Thiago Cordeiro, who guided me during the development of this work. I am also thankful to other professors of the Instituto de Computação who played major roles in my graduation, professor Ph.D. Ícaro Bezerra and professor M.Sc. Glauber Leite. Lastly, I would like to mention professor Maria do Carmo, who helped me a lot since the beginning of my graduation.

Many thanks to my friends, graduation colleagues, and special people, Rafael, Júlia, Álvaro, Sofia, Luís, Andressa, Eduardo, Arthur, Eduarda, Fernanda, Rodrigo, Hegel, and Liz, who accompanied me and gave me support on this path.

Finally, words cannot express my gratitude to my family, especially my parents. I would not have come this far without them.

“Do. Or do not. There is no try.”

– Yoda

Resumo

Dispositivos de assistência ventricular são bombas mecânicas usadas como suporte para pacientes com insuficiência cardíaca. Esses dispositivos são um grande objeto de pesquisa no campo da engenharia biomédica, com foco no control de sistemas fisiológicos com o objetivo de melhorar a performance desses dispositivos. Pesquisadores da Universidade Federal de Alagoas têm investigado diversas estratégias de controle aplicadas a eles há anos. Nessas investigações anteriores, um modelo numérico do coração esquerdo foi utilizado com sucesso para performar simulações de controle. Entretanto, para que se obtenham resultados ainda mais acurados, um modelo mais complexo é necessário. Esse trabalho desenvolve um *framework* de um modelo do sistema cardiovascular humano que considera ambos os lados do coração e outras variáveis hemodinâmicas. Esse *framework* permite que um dispositivo de assistência ventricular seja acoplado a ele e controlado. Como prova de conceito, o modelo numérico foi inteiramente simulado utilizando um script em MATLAB[®] e obteve uma boa performance com um controlador *Starling-like*, que é uma técnica de controle que usa variáveis do modelo desenvolvido, como o fluxo da bomba e a pressão ventricular esquerda final diastólica. As simulações alcançaram os resultados esperados e o código *open source* desse *framework* está disponível para download.

Palavras-chave: modelo do sistema cardiovascular; dispositivo de assistência ventricular; sistemas fisiológicos; controle starling-like; engenharia biomédica.

Abstract

Ventricular assist devices are mechanical pumps used as support to patients with heart failure. These devices are a great object of research in the biomedical engineering field, with focus on physiological control systems in order to improve the performance of these devices. Researchers at the Universidade Federal de Alagoas have investigated several control strategies applied to them for years. In these previous investigations, a left heart numerical model was successfully used to perform control simulations. However, in order to have even more accurate results, a more complex model is necessary. This work develops a human cardiovascular system model framework that considers both sides of the heart and other hemodynamical variables. This framework allows a ventricular assist device to be coupled to it and controlled. As a proof of concept, the entire numerical model was simulated using a script in MATLAB[®] and performed well with a Starling-like controller, which is a control technique that uses variables from the developed model, such as the pump flow and the left-ventricular end-diastolic pressure. The simulations reached the expected results and the open source code of this framework is available to download.

Keywords: cardiovascular system model; ventricular assist device; physiological systems; starling-like control; biomedical engineering.

Contents

List of Acronyms	vi
List of Figures	viii
1 Introduction	1
1.1 Motivation	1
1.2 Objectives	2
1.3 Structure	2
2 Cardiovascular Model	3
2.1 The Human Cardiovascular System	3
2.1.1 The Anatomy of the Human Heart	3
2.1.2 The Cardiac Cycle	4
2.2 Model of the Human Cardiovascular System	7
2.2.1 Lumped Parameters Cardiovascular Model	7
2.2.2 Model simulation and validation	19
2.3 Final Considerations	24
3 Ventricular Assist Devices	26
3.1 Ventricular Assist Devices	26
3.2 The LVAD Model	28
3.3 LVAD+CVS model simulation and validation	31
3.4 Final Considerations	33
4 An Immediate Response Starling-Like Controller	34
4.1 Starling-Like Control	34
4.2 Controller Simulation and Validation	37
4.3 Final Considerations	42
5 Conclusion	43

List of Acronyms

BTC	<i>Bridge-To-Candidacy</i>
BTD	<i>Bridge-To-Decision</i>
BTR	<i>Bridge-To-Recovery</i>
BTT	<i>Bridge-To-Transplant</i>
CF	<i>Continuous Flow</i>
CL	<i>Control Line</i>
CO	<i>Cardiac Output</i>
CRC	<i>Cardiac Response Curve</i>
CSC	<i>Constant Speed Control</i>
CVS	<i>Cardiovascular System</i>
CVD	<i>Cardiovascular Disease</i>
DT	<i>Destination Therapy</i>
ECG	<i>Electrocardiogram</i>
EDV	<i>End-Diastolic Volume</i>
EF	<i>Ejection Fraction</i>
ESV	<i>End-Systolic Volume</i>
ESPVR	<i>End-Systolic Pressure-Volume Relationship</i>
HF	<i>Heart Failure</i>
HR	<i>Heart Rate</i>
LVAD	<i>Left Ventricular Assist Device</i>
MAP	<i>Mean Arterial Pressure</i>
RVAD	<i>Right Ventricular Assist Device</i>
SLC	<i>Starling-Like Controller</i>
SV	<i>Stroke Volume</i>
SVR	<i>Systemic Vascular Resistance</i>
VAD	<i>Ventricular Assist Device</i>

List of Figures

1	Human heart structure.	4
2	Cardiac cycle events on the left side of the human heart.	5
3	Pressure-volume diagram.	6
4	1D model of any artery.	8
5	Electrical circuit analogous to the hydraulic system shown in Figure 4.	10
6	Model of a heart valve as an electrical circuit.	11
7	Left atrial and ventricular elastances obtained by computer simulation using MATLAB®.	13
8	Lumped parameter cardiovascular model.	14
9	Cardiovascular model with the addition of compliance in the aorta. The red dashed line shows this insertion.	15
10	Excerpts from the cardiovascular models before and after modification.	15
11	Comparison of magnitudes and phases before and after modification.	16
12	Magnitudes and phases before and after the modification with emphasis on a smaller interval.	17
13	Left Heart simulated curves.	21
14	Right Heart simulated curves.	22
15	Thoratec’s Heartmate I® (left) and Heartmate II® (right).	27
16	Heartmate II.	28
17	LVAD model attached to the cardiovascular model.	29
18	Pump speed linearly increasing and its respective behavior.	32
19	Pump speed (a) and pump flow for different values of SVR (b)-(f).	33
20	Starling’s Law.	35
21	Operating point trajectory on changing preload conditions.	35
22	Block Diagram of the physiological control system.	37
23	Left-ventricular end-diastolic pressure and the resistance of the mitral valve through time with the increase of P_{lved} at 12 seconds.	38
24	Mean measured flow and mean target flow comparison through time, showing how the controller worked after increase P_{lved} at 12 seconds.	38
25	Pump flow and pump speed vary according to the controller. The speed increases with the increase of P_{lved}	39

26	Operating point trajectory. Before the disturbance, it is located on the triangle point. Then, the increase in the preload conditions pulls it to the right side of the CL, and the controller brings it back to the CL (on the circle point).	39
27	Left-ventricular end-diastolic pressure and the resistance of the mitral valve through time with the decrease of P_{lved} at 12 seconds.	40
28	Mean measured flow and mean target flow comparison through time, showing how the controller worked after decrease P_{lved} at 12 seconds.	40
29	Pump flow and pump speed vary according to the controller. The speed decreases with the decrease of P_{lved}	41
30	Operating point trajectory. Its initial position is the triangle point. Then, the decrease in the preload conditions pulls it to the left side of the CL, and the controller brings it back to the CL (on the circle point).	41

1

Introduction

1.1 Motivation

According to World Health Organization, cardiovascular diseases (CVDs) are the leading cause of death worldwide. In 2019, about 17.9 million people died from CVDs, representing 32% of all deaths globally. Of these deaths, 85% were caused by strokes, and heart attacks [1].

Guyton and Hall define heart failure (HF) as the reduction of the ability of the heart to pump enough blood to the body [2]. Ventricular assist devices (VADs) are mechanical devices usually used to support end-stage patients with HF. These devices can be a bridge treatment for these patients while they await heart transplantation or can be used as a destination therapy [3]. Furthermore, these devices demand control techniques to better attend to patient condition changes. These control techniques are proposed to avoid some adverse effects, such as major bleeding, or onset suction [4].

To validate the control techniques, *in silico* simulations are essential to these studies in order to avoid *in vivo* experiments and when *in vitro* simulation is not possible. Consequently, modeling biological systems is a crucial piece of the biomedical engineering field. In the Instituto de Computação at the Universidade Federal de Alagoas, research related to modeling the cardiovascular system (CVS) has been introduced previously in [5, 6, 7]. In these previous works, a left heart lumped parameter model was used based on the one proposed by [8], and it was proved to be a robust model for these studies. Despite that, it has some limitations once it considers only the left side of the human heart. For instance, if a control technique is applied to a Left Ventricular Assist Device (LVAD) coupled to this model, it is impossible to study how this controller affects other parts of the CVS, such as the right heart and the pulmonary arterial and venous circulations. Considering this, it would be helpful to have a more comprehensive CVS model that considers both sides of the heart and other circulatory system variables.

1.2 Objectives

The main objective of this work is to provide a new framework for a lumped parameter CVS model that allows the coupling of VAD numerical models and the application of more complex control techniques. To achieve that, the following specific objectives were proposed:

1- To study papers with different lumped parameter CVS models and choose one representing both sides of the heart and other physiological parameters.

2 - To extract the first-order differential equations of the lumped parameters model chosen and simulate it using software, making some adaptations if necessary.

3 - To do the coupling of a left ventricular assist device model with the CVS model, simulating and validating it.

4 - To choose a control technique and apply it to the LVAD model to prove that this system can be used for control purposes.

Finally, this work should present a framework that must be used in future research, expanding the possibilities of studying different sections of the cardiovascular system. Besides, it is expected to be a legacy to future researchers at the Universidade Federal Alagoas and any others who may find this work helpful.

1.3 Structure

This work consists of five chapters. Chapter 2 begins with an introduction to basic physiological concepts about the cardiovascular system. Then, it explains the different types of CVS models, focusing on the 0D modeling, which is the one used in this work. Finally, it will present and validate the model used in the framework proposed here. Chapter 3 focus on ventricular assist devices. It explains the different generations of VADs and brings the model of rotatory LVAD used in this work. Besides that, this chapter shows the results of the simulations of this model and validates it. Chapter 4 introduces the Starling-like control, the controller chosen for this work. It will explain the concept behind this type of controller and prove that the framework can be controlled. Finally, chapter 5 discusses all the work with a final conclusion.

2

Cardiovascular Model

In this chapter, basic concepts about the human cardiovascular system will be presented, such as the anatomy of the human heart, the cardiac cycle, pressure-volume diagram, among others. Concepts about modeling systems in the time domain will also be discussed, with an introduction to representation in state space. A lumped parameter model of the CVS will be presented, which will be represented as an electrical circuit. Finally, the computer simulation results of this lumped parameter model will be shown through pressure, flow, and volume curves, in addition to other estimates collected from these results.

2.1 The Human Cardiovascular System

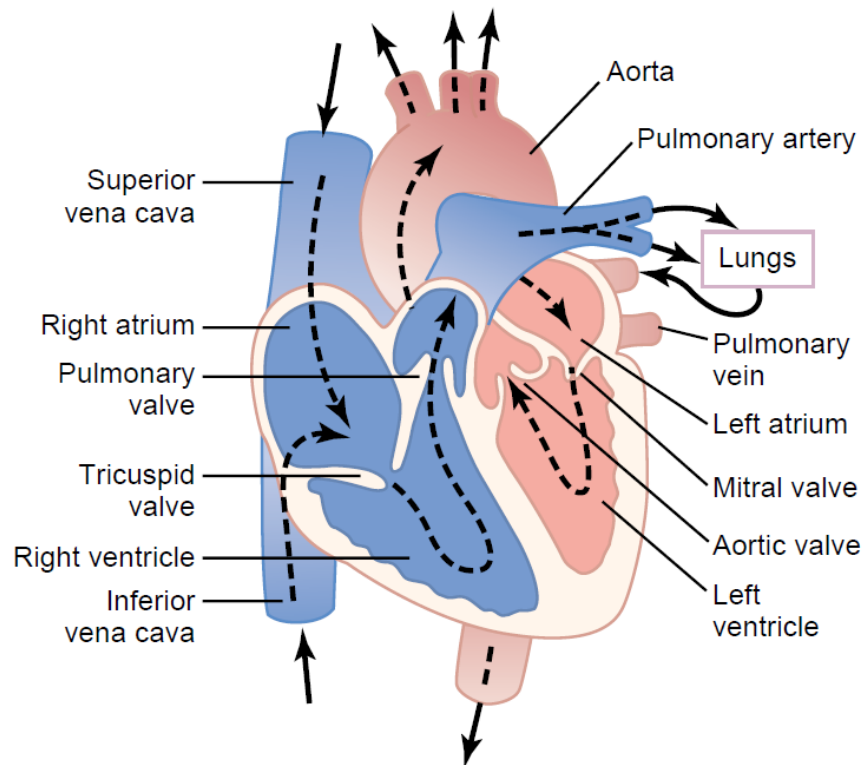
This section will present an overview of CVS, introducing basic concepts about the anatomy of the heart, the cardiac cycle, and its stages: systole and diastole, which are essential for understanding the rest of the work.

2.1.1 The Anatomy of the Human Heart

According to [2], the human heart is formed by two distinct pulsatile pumps: a right heart, which pumps blood to the lungs, and a left heart, which pumps blood to peripheral organs. Each of these pumps comprises two chambers: an atrium and a ventricle.

Each atrium works as a primer pump, which drives blood to the corresponding ventricle, which serves as the main pumping force for blood, sending it to the pulmonary circulation, in the case of the right ventricle, and to the peripheral circulation, in the case of the left.

Figure 1: Human heart structure.



Note. Reprinted from *Textbook of Medical Physiology* (p.104), by A.C. Guyton and J.E. Hall, 2015, Elsevier. Copyright 2006 by Elsevier.

This is illustrated in Figure 1, where the anatomy of the human heart and blood circulation through the chambers mentioned above are shown. It is possible to observe that the blood reaches the right atrium from the superior and inferior vena cava, then passes to the right ventricle through the opening of the tricuspid valve, where it is sent to the lungs through the pulmonary valve. Then, the blood returns to the heart through the pulmonary veins, reaching the left atrium, which drives it to the left ventricle through the mitral valve. Finally, the blood passes through the aortic valve to the aorta, distributed to the peripheral organs.

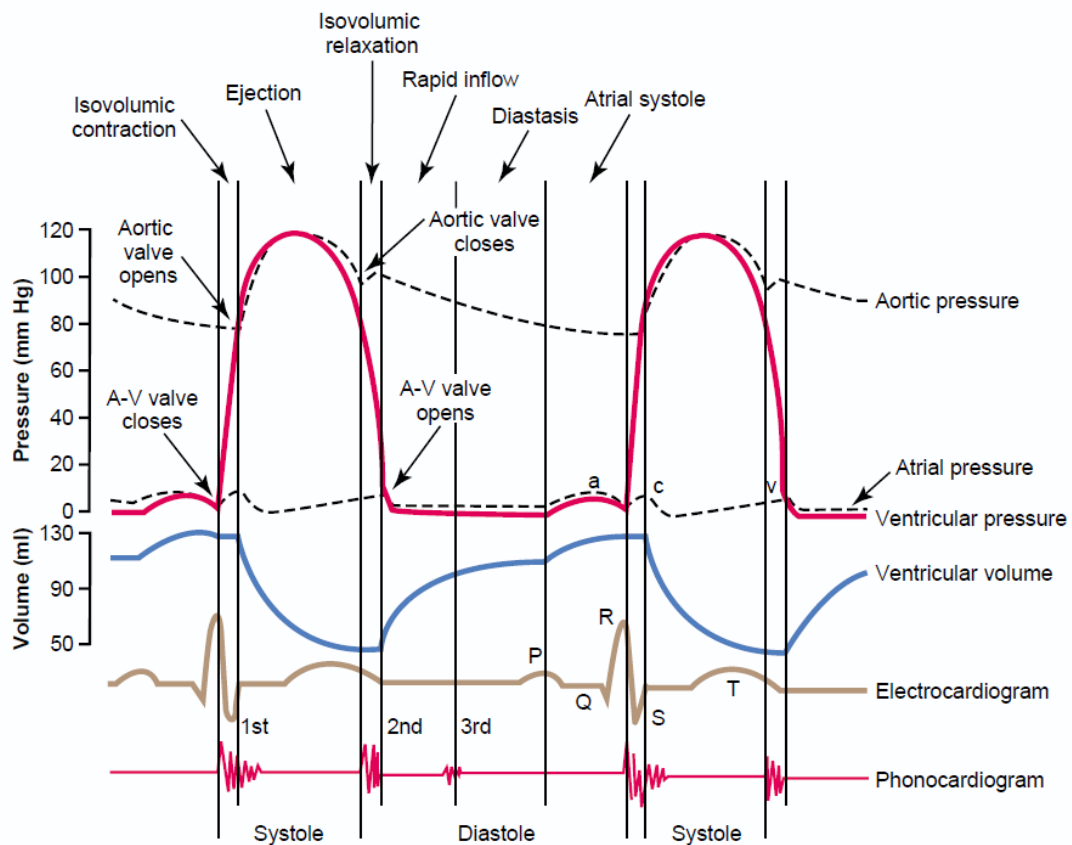
2.1.2 The Cardiac Cycle

The cardiac cycle is defined as the series of events between two consecutive heartbeats, where each cycle is initiated by the spontaneous generation of an electrical potential that diffuses first to the atria and subsequently to the ventricles [2]. A delay in the cardiac impulse passage from the atria to the ventricles causes an initial contraction in the atria, pumping the blood inside the atria to the ventricles.

Thus, the cardiac cycle is divided into two stages: systole and diastole. Diastole is the period of relaxation, where the heart fills with blood, while systole is the period of contraction, where the heart expels blood.

The duration of a cardiac cycle is inversely proportional to the heart rate. For example, if the heart rate is 72 bpm, then the duration of a cardiac cycle is equal to 0.833 s.

Figure 2: Cardiac cycle events on the left side of the human heart.



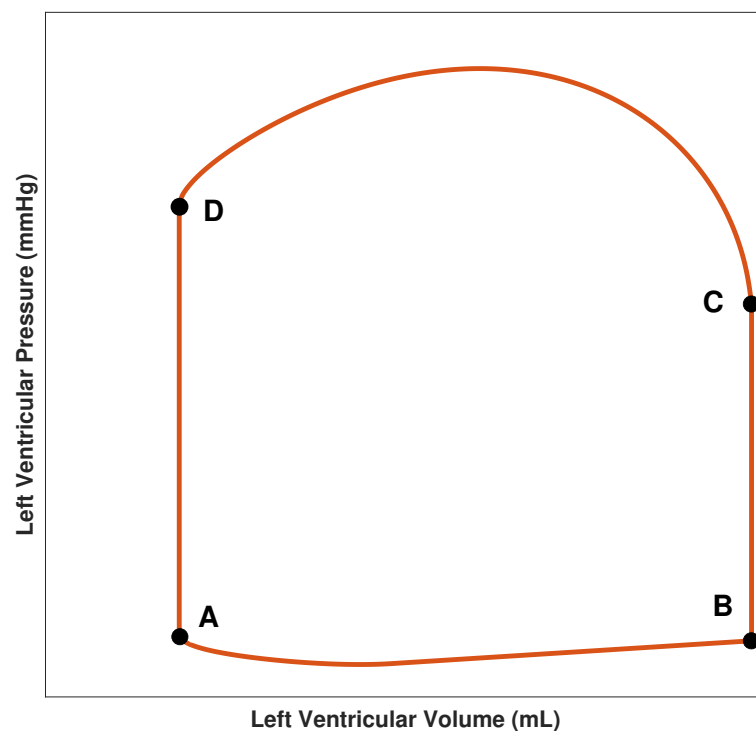
Note. Reprinted from *Textbook of Medical Physiology* (p.107), by A.C. Guyton and J.E. Hall, 2015, Elsevier. Copyright 2006 by Elsevier.

In Figure 2, the events that occur during the cardiac cycle within the stages of systole and diastole on the left side of the human heart are shown. With it, it can be seen that systole begins with the opening of the aortic valve when blood is sent into the peripheral circulation through the aorta. With this ejection, the aortic and ventricular pressures reach their peaks, while there is a decay in the ventricular volume. Furthermore, since blood is pumped out of it, the atrial pressure goes through a gentle decay and then through a near plateau state. The systole is then terminated with the closing of the aortic valve. After that, the heart enters the period of isovolumetric relaxation, in which there is a decrease in ventricular pressure.

In turn, diastole begins with the mitral (or bicuspid) valve opening, the moment when the ventricle fills. This can be seen in the Figure 2 by observing an increase in ventricular volume while the ventricular pressure decreases and, together with the atrial pressure, goes through a moment in which it remains almost constant until, near the end of this period, when there is a smooth increase in both. The diastole is then completed with the closing of the mitral valve.

After it and before systole, there is the period of isovolumetric contraction, where the increase in pressures in the atrium and ventricle begins since it is where the muscle contraction that will cause the ejection period begins.

Figure 3: Pressure-volume diagram.



In Figure 3 are the cited periods of the cardiac cycle through the pressure-volume diagram, which demonstrates the volume and pressure relationships in the left ventricle. In point A (mitral valve opening), there is the beginning of the filling period, where there is an increase in volume and constancy of pressure until there is a slight increase when approaching point B (mitral valve closing). From this point on, there is a significant increase in ventricular pressure while the volume remains constant. From point C (opening of the aortic valve) to point D (closing of the aortic valve), there is a decrease in volume simultaneously with an increase in pressure, which will begin to fall only when very close to the valve closure. Finally, there is the return from point D to point A, where the pressure will decrease while the volume remains constant.

Figure 2 also shows the electrocardiogram (ECG) signal during the cardiac cycle on the left side of the heart. The set of waves shown in the figure, which form the ECG, is composed of P, Q, R, S, and T waves. These waves are electrical voltages generated by the heart that can be measured using an electrocardiograph. The P wave is produced when atrial contraction occurs, while the set formed by the Q, R, and S waves, called the *QRS* complex, when ventricular contraction starts. Finally, the T wave is generated at the end of ventricular contraction.

2.2 Model of the Human Cardiovascular System

This section aims to introduce the concept of 0D CVS models. Beginning with a brief explanation of the possible model types of representation of the CVS. Then, the modeling of the CVS elements, such as valves, pressures, and blood streams, is explained. Also, the concept of the elastance function is shown, and the CVS model used in this work is presented. Finally, the results of a computer simulation of this model are presented.

2.2.1 Lumped Parameters Cardiovascular Model

The choice of an appropriate CVS model is an essential factor in bioengineering so that simulations and research can be carried out and contemplated as much as possible in real physiological situations. Thus, various degrees on the complexity of cardiovascular models can be considered in a study, where the suitable one must meet the desired prerequisites for the work.

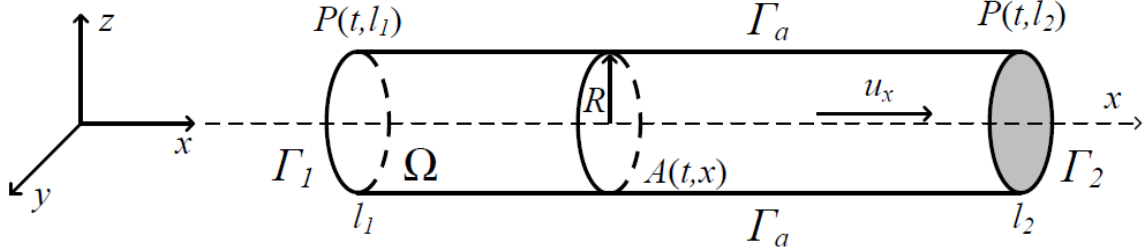
According to [9], multi-level geometric modeling can solve the issue of model complexity since this modeling covers several levels of accuracy of different parts of the CVS. At the top of the hierarchy of these levels of accuracy is the 3D modeling of the CVS, which has the highest degree of complexity and most accurately describes the behavior of the hemodynamic variables in the CVS. 1D models, on the other hand, reduce the system's complexity to just one axis, representing the direction of blood flow. Finally, 0D modeling is derived from 1D and can reproduce global CVS behaviors such as pressures, flows, and volumes.

Thus, this study will use a lumped parameters model, also known as the 0D model. It has less complexity than the others and still efficiently represents the dynamics of the human cardiovascular system, facilitating its computational simulation once it is modeled as an electrical circuit. In this way, it is easy to make analogies between this type of system and hydraulic systems, as is the case of 1D models. In addition, representations via electrical circuits allow the use of classical circuit analysis techniques, such as Kirchhoff's laws.

As stated in [9], analogies can be made between: blood pressure and electric voltage, blood flow and electric current. Electronic elements such as resistors, inductors, and capacitors will describe blood vessels' friction, inertia, and elasticity behaviors, respectively.

Figure 4 represents a 1D model of any given cylindrical artery with domain region Ω and boundary conditions Γ_a representing the physical walls of the artery. Γ_1 and Γ_2 represent, respectively, the boundary conditions referring to the remainder of the circulatory system and the inflow and outflow interfaces.

Figure 4: 1D model of any artery.



Note. Reprinted from *Sistema de Controle Fisiológico Aplicado a Dispositivos de Assistência Ventricular* by T. D. Cordeiro, 2017.

The total length of the artery, which is plotted on the x -axis, is given by l . The artery is bounded by l_1 and l_2 , where $l_1 \leq x \leq l_2$. Considering the cylindrical shape of the artery, we have that its cross-sectional area is $A(t, x) = \pi R^2(t, x)$, where $R(t, x)$ is the radius of the cylinder. The velocity profile of the blood flow in the artery in the x direction is given by u_x . According to [10], the mathematical model representing the blood flow in this artery is given by the system in 1.

$$\begin{cases} \frac{\partial A}{\partial t} + \frac{\partial Q}{\partial x} = 0 \\ \frac{\partial Q}{\partial t} + \alpha \frac{\partial}{\partial x} \left(\frac{Q^2}{A} \right) + \frac{A}{\rho} \frac{\partial P}{\partial x} + K_R \frac{Q}{A} = 0 \end{cases} \quad (1)$$

With $x \in (0, l), t \in (0, T], Q_1(t) = Q(t, 0), P_1(t) = P(t, 0), Q_2(t) = Q(t, l)$ and $P_2(t) = P(t, l)$. Where $Q(t, l)$ is the volumetric flow through cross section A given by Equation 2, α (flow momentum correction coefficient), ρ (blood density), and K_R (friction parameter) are constants.

$$Q(t, x) := \int_{A(t, x)} u_x d\sigma \quad (2)$$

Furthermore, a third equation is needed once the system has three variables. Equation 3 shows the displacement of the artery walls η concerning pressure P , where P_{ext} and A_0 are constants representing pressure and area reference, respectively. And $\beta_0 = \frac{A_0 c}{\sqrt{\beta_0}}$, c a constant, is related to the physical properties of the vascular tissue.

$$P = P_{ext} + \beta_0 \frac{\sqrt{A} - \sqrt{A_0}}{A_0} \quad (3)$$

From this, one can extract the 0D model derived from the 1D modeling with the earlier equations. For the same artery as in Figure 4, one has that

$$\frac{\partial A}{\partial t} \approx 2\pi R_0 \frac{\partial \eta}{\partial t} \quad (4)$$

From which Equation 5 is assumed with $k_1 = \frac{3\pi R_0^3}{2Eh}$, where h is the thickness of the vascular tissue and E is Young's modulus.

$$\frac{\partial A}{\partial t} = k_1 \frac{\partial P}{\partial t} \quad (5)$$

It is also necessary to define the mean pressure and the mean volumetric flow rate within the artery, given respectively by Equations 6 and 7.

$$\hat{p} = \frac{1}{l} \int_0^l P dx \quad (6)$$

$$\hat{Q} = \frac{1}{l} \int_0^l Q dx \quad (7)$$

With this, one integrates with respect to x the first equation in 1 as shown in 8. Furthermore, one can substitute $\partial A/\partial t$ as in Equation 5 and then manipulate $\partial P/\partial t$ via Equation 6. The end of this integration is Equation 9.

$$\int_0^l \frac{\partial A}{\partial t} dx + \int_0^l \frac{\partial Q}{\partial t} dx = 0 \quad (8)$$

$$k_1 l \frac{dp}{dt} + Q_2 - Q_1 = 0 \quad (9)$$

Regarding the integration of the second equation in 1, one has the following:

$$\int_0^l \left[\frac{\partial Q}{\partial t} + \alpha \frac{\partial}{\partial x} \left(\frac{Q^2}{A} \right) + \frac{A}{\rho} \frac{\partial P}{\partial x} + K_R \frac{Q}{A} \right] dx = l \frac{d\hat{Q}}{dt} + \alpha \left[\frac{Q_2^2}{A_2} - \frac{Q_1^2}{A_1} \right] + \int_0^l \left[\frac{A}{\rho} \frac{\partial P}{\partial x} + K_R \frac{Q}{A} \right] dx = 0 \quad (10)$$

Also, according to [10], the value of $\left[\frac{Q_2^2}{A_2} - \frac{Q_1^2}{A_1} \right]$ in the Equation 10 is minimal compared to the others and can be discarded. Furthermore, the variation of A at x is also much smaller compared to P and Q . Thus Equation 10 can be approximated as:

$$l \frac{d\hat{Q}}{dt} + \int_0^l \left[\frac{A_0}{\rho} \frac{\partial P}{\partial x} + K_R \frac{Q}{A_0} \right] dx = 0 \quad (11)$$

Which finally results in Equation 12.

$$\frac{\rho l}{A_0} \frac{d\hat{Q}}{dt} + \frac{\rho K_R l}{A_0^2} \hat{Q} + P_2 - P_1 = 0 \quad (12)$$

Now, Equations 9 and 12 are the lumped parameter descriptions of the behavior of the blood flow inside the artery in Figure 4. With this, it is now possible to interpret these equations as those of an electrical circuit through the analogy mentioned earlier between hydraulic systems and electrical circuits.

Regarding Equation 12, by means of analogous systems, $R := \frac{\rho K_R l}{A_0^2}$ as the flow resistance

induced by blood viscosity and $L := \frac{\rho l}{A_0}$ as the inductance of the flow being the inertia term in the law of conservation of momentum. In Equation 9, one assumes $C := k_1 l$ as the compliance of the artery, which represents the mass storage coefficient in the law of conservation of masses. The result is given in Equation 13.

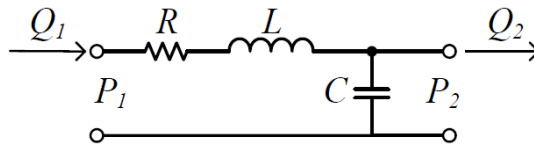
$$\begin{cases} C \frac{d\hat{p}}{dt} + Q_2 - Q_1 = 0 \\ L \frac{d\hat{Q}}{dt} + R\hat{Q} + P_2 - P_1 = 0 \end{cases} \quad (13)$$

Now, one assumes, for instance, that P_1 and Q_2 are given. Moreover, from 13 one has four variables and two equations, so it is necessary to make some additional assumptions. Since the dynamics of the system is given by the time-differentiable variables \hat{p} and \hat{Q} , one approximate $\hat{p} \approx P_2$ and $\hat{Q} \approx Q_1$, where such an approximation is reasonable for a small cylinder. With the previous assumptions, one obtains the system of first-order differentiable equations shown in 14.

$$\begin{cases} C \frac{dP_2}{dt} - Q_1 = -Q_2 \\ L \frac{dQ_1}{dt} + RQ_1 + P_2 = P_1 \end{cases} \quad (14)$$

with Q_1 and P_2 as state variables, which ultimately represents the electrical circuit analogous to the blood vessel shown in Figure 4. Figure 5 shows the representation of this system as an electrical circuit.

Figure 5: Electrical circuit analogous to the hydraulic system shown in Figure 4.



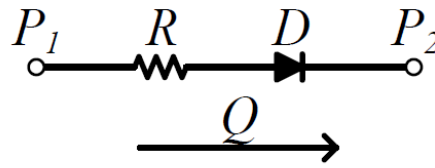
Note. Reprinted from *Sistema de Controle Fisiológico Aplicado a Dispositivos de Assistência Ventricular* by T. D. Cordeiro, 2017.

The present work will use an adaptation of the lumped parameter cardiovascular models in [11] and in [12]. This model consists of the heart's left and right sides, the systemic and pulmonary arterial sections, and the systemic and pulmonary venous sections. It is a tenth-order electrical circuit, meaning ten differentiable elements, including both inductors and capacitors.

As mentioned earlier, the human heart comprises four valves: the mitral, aortic, pulmonary, and tricuspid. These valves open and close, allowing blood flow to circulate between the heart chambers according to the pressure in each chamber. For example, when the pressure in the left atrium is greater than the pressure in the left ventricle, the mitral valve opens, allowing blood to pass from the atrium to the ventricle.

Each heart valve was modeled using an ideal diode in series with a resistor, as shown in Figure 6. For this circuit, the diode's value will be 1 if $P_1 \geq P_2$ and 0 otherwise. This representation is not the most accurate, as it does not account for the possibility of retrograde flow between the chambers before the valves are fully closed. However, it is sufficient for the proposed work. The flow in the circuit in Figure 6 is calculated using the Equation 15.

Figure 6: Model of a heart valve as an electrical circuit.



Note. Reprinted from *Sistema de Controle Fisiológico Aplicado a Dispositivos de Assistência Ventricular* by T. D. Cordeiro, 2017.

$$Q = \frac{D}{R}(P_1 - P_2) \quad (15)$$

Frank and Starling described the heart's contractility as the more the heart muscle is stretched during filling, the greater the force of contraction and the greater the amount of blood pumped through the aorta. This ability of the heart to adapt to increased blood volume is called the Frank-Starling mechanism [2].

The cardiac atria and ventricles were described as contractile chambers in [13], where they have proposed a time-varying function that describes the contractility of these chambers as a relationship between pressure and volume. This function is called the elastance function and is presented according to the Equation 16, where V_0 is a volume constant.

$$E(t) = \frac{P(t)}{V(t) - V_0} \quad (16)$$

Thus, atrial and ventricular pressures will be calculated as relationships between volume and the elastance function. As in [13], Equations 17, 18, 19 and 20 refer to the pressures in the left and right ventricles and the left and right atria, respectively.

$$P_{lv}(t) = E_{lv}(t)(V_{lv}(t) - V_{lv0}) \quad (17)$$

$$P_{rv}(t) = E_{rv}(t)(V_{rv}(t) - V_{rv0}) \quad (18)$$

$$P_{la}(t) = E_{la}(t)(V_{la}(t) - V_{la0}) \quad (19)$$

$$P_{ra}(t) = E_{ra}(t)(V_{ra}(t) - V_{ra0}) \quad (20)$$

In order to calculate the elastance functions, Equation 21 was used for the left ventricle, and the Equation 22 for the atria. These equations are based on the work of [14].

$$E_{lv}(t) = E_{lv,min} + \frac{E_{lv,max} - E_{lv,min}}{2} \cdot \bar{e}_v(t) \quad (21)$$

$$E_a(t) = E_{a,min} + \frac{E_{a,max} - E_{a,min}}{2} \cdot \bar{e}_a(t) \quad (22)$$

The elastance functions are corresponding. Besides, both are normalized by a minimum and a maximum elastance value that multiply an activation function. The right ventricle's elastance is also analogous to that in the left ventricle, and only the constants are changed. The ventricles' activation function is given by the following Equation 23:

$$\bar{e}_v(t) = \begin{cases} 1 - \cos\left(\frac{t}{T_T}\pi\right), & 0 \leq t \leq T_T \\ 1 + \cos\left(\frac{t-T_T}{T_{TE}-T_T}\pi\right), & T_T < t \leq T_{TE} \\ 0, & T_{TE} < t \leq T \end{cases} \quad (23)$$

where T_T represents the peak time of the T wave in the ECG signal, T_{TE} is the end of the T wave, and T is the cardiac period. In turn, the activation function for the elastance in the atria is calculated according to Equation 24:

$$\bar{e}_a(t) = \begin{cases} 0, & 0 \leq t \leq T_{PB} \\ 1 - \cos\left(\frac{t-T_{PB}}{T_{PE}-T_{PB}}2\pi\right), & T_{PB} < t \leq T_{PE} \\ 0, & T_{PE} < t \leq T \end{cases} \quad (24)$$

where T_{PB} is the P wave onset time, T_{PE} is the P wave end time, and, as in the previous activation function, T is the cardiac period time. The same elastance function was used for both atria, so that $E_{la}(t) = E_{ra}(t) = E_a(t)$.

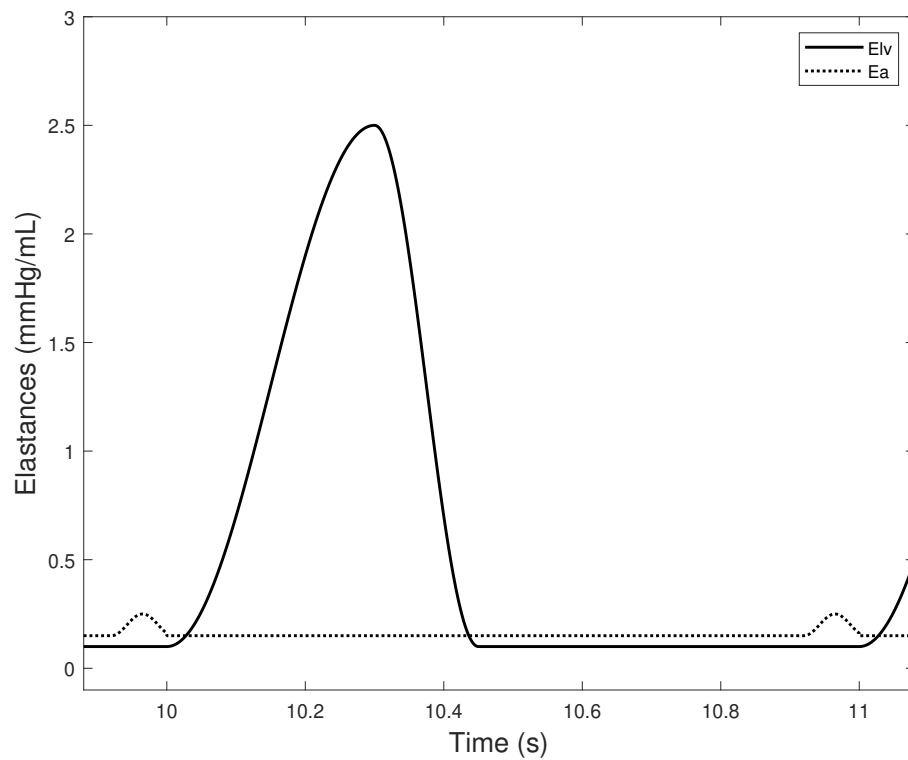
The elastances were computationally simulated through a MATLAB[®] script. In the simulation, the parameters shown in the table 2.1 were used for the function normalization constants and the ECG signal times, which are proportional to the cardiac period.

Table 2.1: Elastance functions parameters.

Parameter	Value
$E_{lv,min}$	0.1000
$E_{lv,max}$	2.5000
$E_{rv,min}$	0.0250
$E_{rv,max}$	1.1500
$E_{a,min}$	0.1500
$E_{a,max}$	0.2500
T_{PB}	0.9200
T_{PE}	1.0100
T_T	0.3000
T_{TE}	0.4500

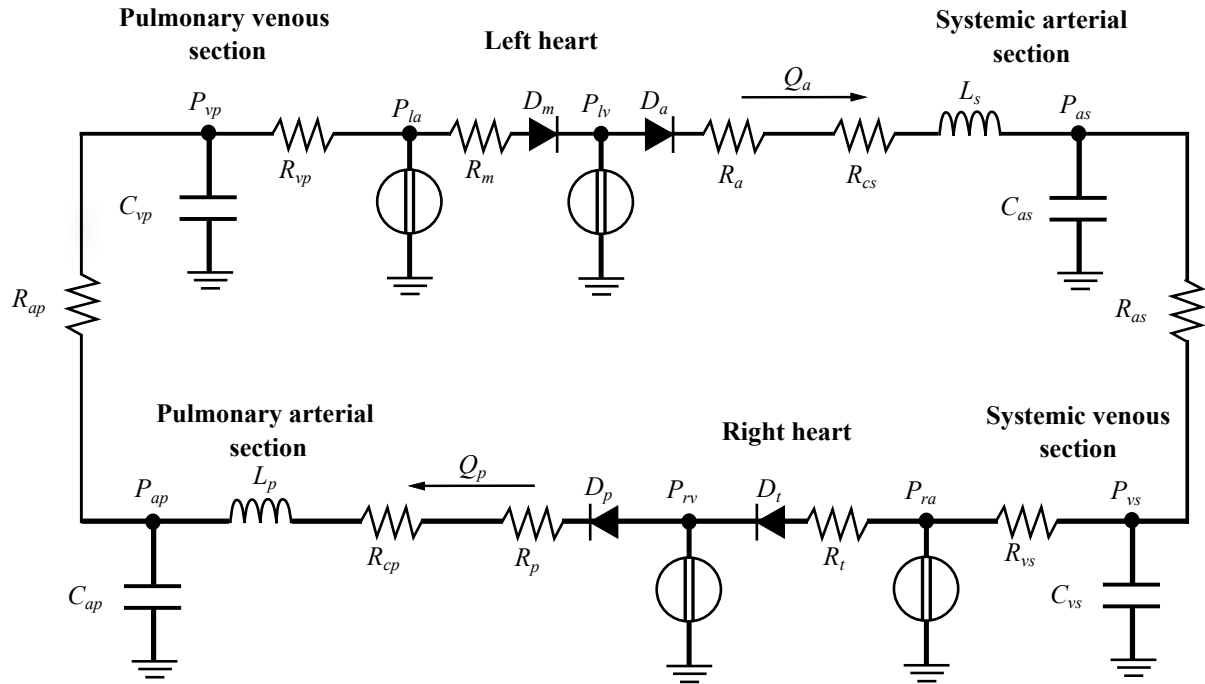
The results of this computational simulation are depicted in Figure 7.

Figure 7: Left atrial and ventricular elastances obtained by computer simulation using MATLAB®.



The model of the human cardiovascular system used here is based on that developed by [11]. It is a parameter-concentrated model that covers the left and right hearts, the systemic arterial and venous sections, and the pulmonary arterial and venous sections.

Figure 8: Lumped parameter cardiovascular model.

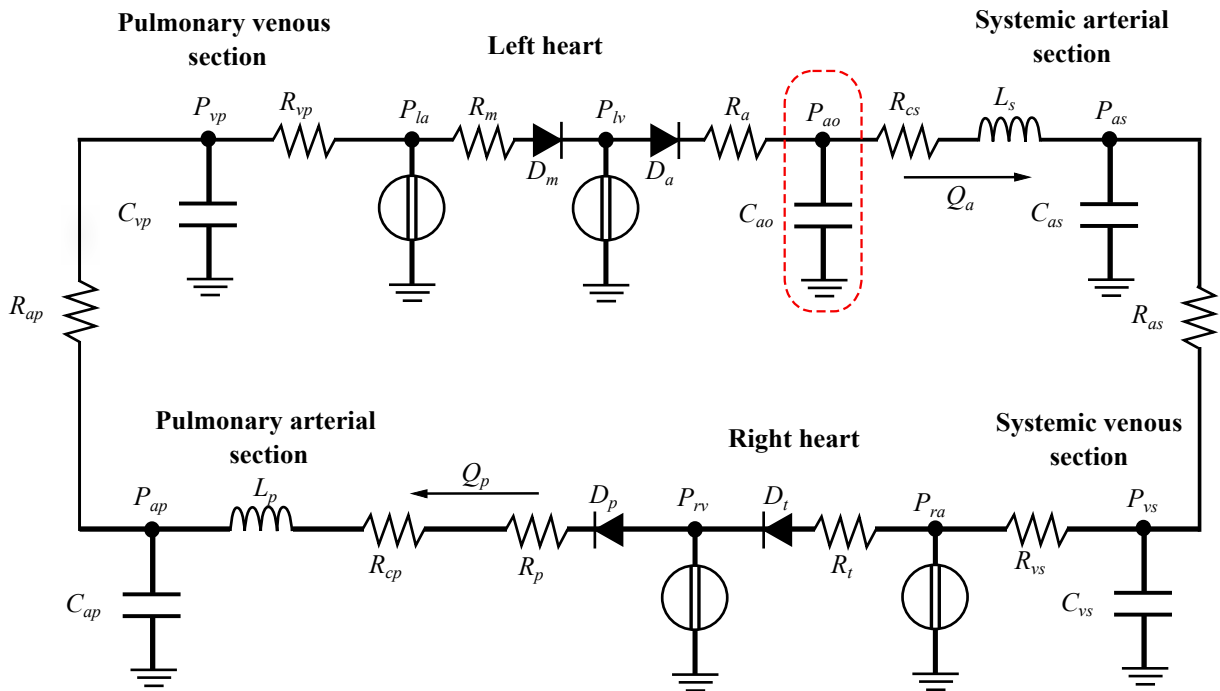


Note. Adapted from *Use of a comprehensive numerical model to improve biventricular pacemaker temporization in patients affected by heart failure undergoing to CRT-D therapy*, by A. Di Molfetta et al., 2010, *Medical & Biological Engineering & Computing*, Volume 48.

Figure 8 shows the electrical circuit analogous to the 0D numerical model, where the systemic venous (pulmonary) section is represented by a resistance R_{vs} (R_{vp}) and a compliance C_{vs} (C_{vp}); the systemic (pulmonary) arterial section is represented by a characteristic resistance R_{cs} (R_{cp}), an inductance L_s (L_p), a compliance C_{as} (C_{ap}) and a peripheral resistance R_{as} (R_{ap}); the atria and ventricles are represented as a pressure (voltage) generator, with the valves represented as an ideal diode in series with a resistance (D_m and R_m ; D_a and R_a ; D_t and R_t ; D_p and R_p); Q_a is the aortic flow, and Q_p is the pulmonary flow; intrathoracic pressure was not taken into account in this model.

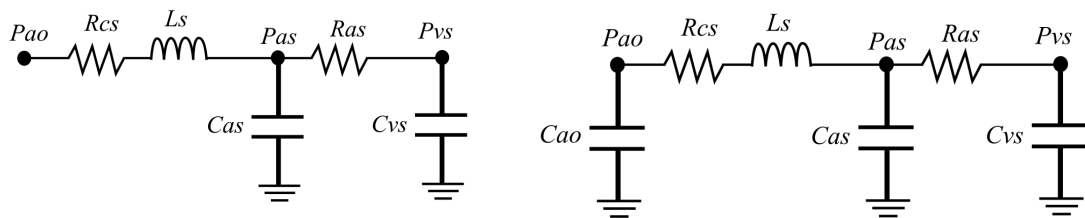
However, the presented model has no compliance in the aorta. Since later a ventricular assist device will be attached to the model and considering that for the left side, this device connects in the left ventricle and the aorta, a modification in the model presented in Figure 8 was performed, and compliance was added in the aorta, as shown in Figure 9. This modification will add a state variable to the system and reduce the complexity of calculating the differential equations after coupling the VAD.

Figure 9: Cardiovascular model with the addition of compliance in the aorta. The red dashed line shows this insertion.



So, to demonstrate that this addition does not harm the overall system behavior, a frequency analysis was performed on the input hydraulic impedance based on the work of [15]. Figure 11(a) shows the circuit section analyzed before the compliance insertion, and Figure 11(b) shows the same section after this insertion.

Figure 10: Excerpts from the cardiovascular models before and after modification.



(a) Original model.

(b) Model with the addition of aortic compliance.

Next, Equation 25 shows the calculated impedance in the original circuit, while Equation 26 shows the impedance of the modified circuit. Figure 11 shows the magnitude and phase in the frequency domain of the two calculated impedances.

$$Z_o = R_{cs} + sL_s + \left(\frac{1}{sC_{as}} \right) \parallel \left(R_{as} + \frac{1}{sC_{vs}} \right) \quad (25)$$

$$Z_M = \left(\frac{1}{sC_{ao}} \right) \parallel \left[R_{cs} + sL_s + \left(\frac{1}{sC_{as}} \right) \parallel \left(R_{as} + \frac{1}{sC_{vs}} \right) \right] \quad (26)$$

Figure 11: Comparison of magnitudes and phases before and after modification.

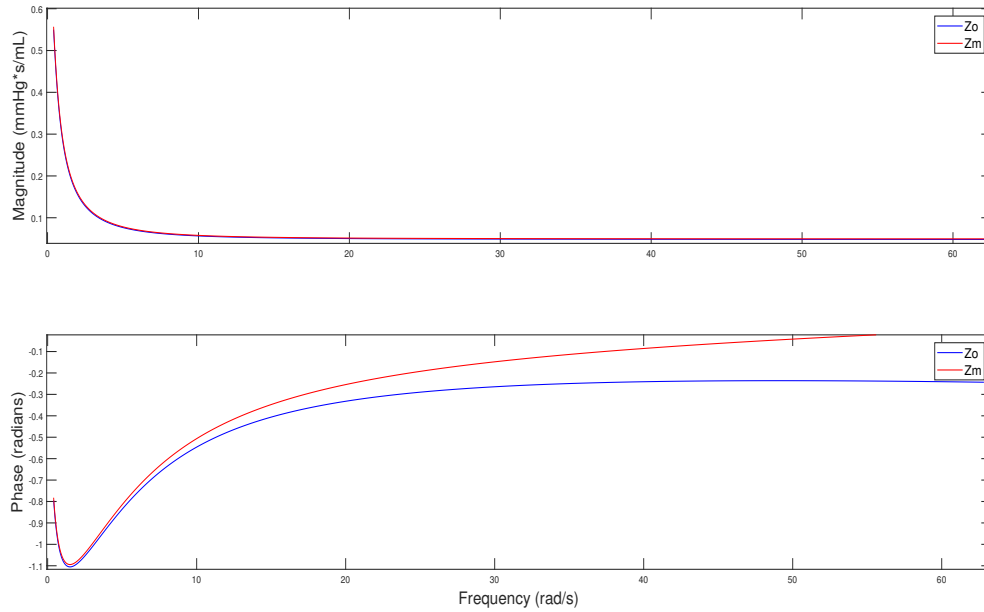
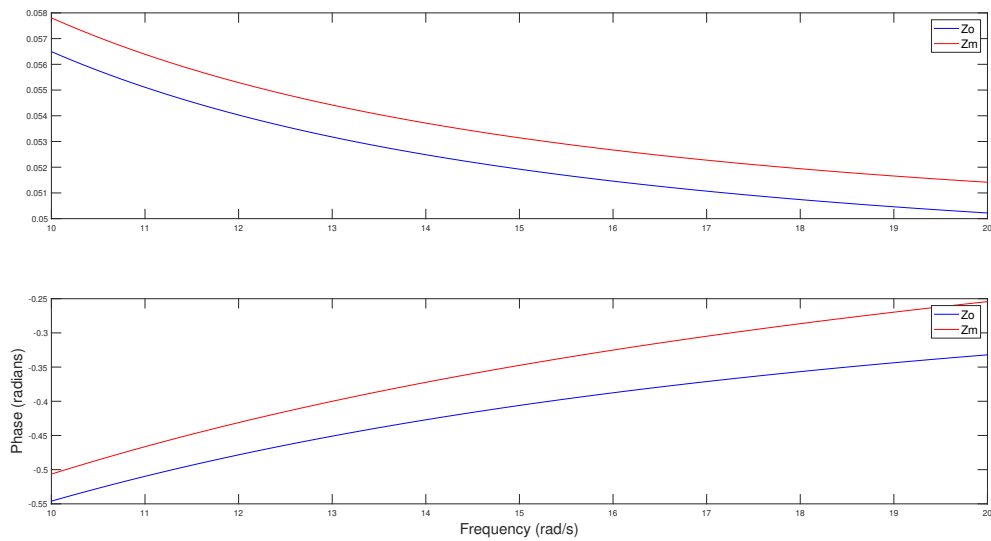


Figure 12 shows the same curves as the previous figure but in a smaller frequency interval so that it can be observed that the difference between the behavior of the circuits is minimal. With this, it is possible to conclude that the general behavior of the system is maintained. Thus the model with compliance in the aorta will be used, and the system to be analyzed is now an eleventh-order system.

Figure 12: Magnitudes and phases before and after the modification with emphasis on a smaller interval.



For the numerical representation of the model, a circuit analysis was performed on the electrical circuit in Figure 9, where Kirchhoff's laws were used to extract the first-degree differential equations of the system. Since this is an eleventh-order system, eleven equations were deduced from the circuit representing the SCH. These equations are shown below:

- **Left Atrial Volume** ($\dot{V}_{la}(t)$)

$$\begin{aligned} \dot{V}_{la}(t) = & - \left[\frac{1}{R_{vp}} + \frac{D_m}{R_m} \right] E_{la}(t) V_{la}(t) + \frac{D_m}{R_m} E_{lv}(t) V_{lv}(t) + \frac{P_{vp}(t)}{R_{vp}} \\ & + \left[\frac{1}{R_{vp}} + \frac{D_m}{R_m} \right] E_{la}(t) V_{la0} - \frac{D_m}{R_m} E_{lv}(t) V_{lv0} \end{aligned} \quad (27)$$

- **Left Ventricular Volume** ($\dot{V}_{lv}(t)$)

$$\begin{aligned} \dot{V}_{lv}(t) = & \frac{D_m}{R_m} E_{la}(t) V_{la}(t) - \left[\frac{D_m}{R_m} + \frac{D_a}{R_a} \right] E_{lv}(t) V_{lv}(t) + \frac{D_a}{R_a} P_{ao}(t) \\ & - \frac{D_m}{R_m} E_{la}(t) V_{la0} + \left[\frac{D_m}{R_m} + \frac{D_a}{R_a} \right] E_{lv}(t) V_{lv0} \end{aligned} \quad (28)$$

- **Aortic Pressure** ($\dot{P}_{ao}(t)$)

$$\dot{P}_{ao}(t) = \frac{D_a}{R_a C_{ao}} E_{lv}(t) V_{lv}(t) - \frac{D_a}{R_a C_{ao}} P_{ao}(t) - \frac{Q_a(t)}{C_{ao}} - \frac{D_a}{R_a C_{ao}} E_{lv}(t) V_{lv0} \quad (29)$$

- **Arterial Flow** ($\dot{Q}_a(t)$)

$$\dot{Q}_a(t) = \frac{P_{ao}(t)}{L_s} - \frac{R_{cs}}{L_s} Q_a(t) - \frac{P_{as}(t)}{L_s} \quad (30)$$

- **Systemic Pressure** ($\dot{P}_{as}(t)$)

$$\dot{P}_{as}(t) = \frac{Q_a(t)}{C_{as}} - \frac{P_{as}(t)}{R_{as}C_{as}} + \frac{P_{vs}(t)}{R_{as}C_{as}} \quad (31)$$

- **Systemic Venous Pressure** ($\dot{P}_{vs}(t)$)

$$\dot{P}_{vs}(t) = \frac{P_{as}(t)}{R_{as}C_{vs}} - \left[\frac{1}{R_{as}} + \frac{1}{R_{vs}} \right] \frac{P_{vs}(t)}{C_{vs}} + \frac{E_{ra}(t)V_{ra}(t)}{R_{vs}C_{vs}} - \frac{E_{ra}(t)V_{ra0}}{R_{vs}C_{vs}} \quad (32)$$

- **Right Atrial Volume** ($\dot{V}_{ra}(t)$)

$$\begin{aligned} \dot{V}_{ra}(t) = & - \left[\frac{1}{R_{vs}} + \frac{D_t}{R_t} \right] E_{ra}(t)V_{ra}(t) + \frac{D_t}{R_t} E_{rv}(t)V_{rv}(t) + \frac{P_{vs}(t)}{R_{vs}} \\ & + \left[\frac{1}{R_{vs}} + \frac{D_t}{R_t} \right] E_{ra}(t)V_{ra0} - \frac{D_t}{R_t} E_{rv}(t)V_{rv0}(t) \end{aligned} \quad (33)$$

- **Right Ventricular Volume** ($\dot{V}_{rv}(t)$)

$$\begin{aligned} \dot{V}_{rv}(t) = & \frac{D_t}{R_t} E_{ra}(t)V_{ra}(t) - \frac{D_t}{R_t} E_{rv}(t)V_{rv}(t) - Q_p(t) \\ & + \frac{D_t}{R_t} (E_{rv}(t)V_{rv0} - E_{ra}(t)V_{ra0}) \end{aligned} \quad (34)$$

- **Pulmonary Flow** ($\dot{Q}_p(t)$)

$$\dot{Q}_p(t) = -\frac{P_{ap}(t)}{L_p} - \left[\frac{R_p + R_{cp}}{L_p} \right] Q_p(t) + \frac{E_{rv}(t)V_{rv}(t)}{L_p} - \frac{E_{rv}(t)V_{rv0}}{L_p} \quad (35)$$

- **Pulmonary Pressure** ($\dot{P}_{ap}(t)$)

$$\dot{P}_{ap}(t) = -\frac{P_{ap}(t)}{R_{ap}C_{ap}} + \frac{Q_p(t)}{C_{ap}} + \frac{P_{vp}(t)}{R_{ap}C_{ap}} \quad (36)$$

- **Pulmonary Venous Pressure** ($\dot{P}_{vp}(t)$)

$$\dot{P}_{vp}(t) = \frac{E_{la}(t)V_{la}(t)}{R_{vp}C_{vp}} + \frac{P_{ap}(t)}{R_{ap}C_{vp}} - \left[\frac{1}{R_{ap}} + \frac{1}{R_{vp}} \right] \frac{P_{vp}(t)}{C_{vp}} - \frac{E_{la}(t)V_{la0}}{R_{vp}C_{vp}} \quad (37)$$

2.2.2 Model simulation and validation

With the first-degree differential equations obtained in the previous section, we can have a time-domain modeling of the modified CVS model.

According to [16], the time domain (or state space) approach is a highly advantageous system modeling technique due to its comprehensiveness. It can be used to design and model nonlinear, time-varying systems with non-zero initial conditions, among other advantages.

Thus, a continuous time-variant system can be represented in state space through the differential equations below, which are, respectively, the state equation and the output equation:

$$\dot{\mathbf{x}}(\mathbf{t}) = \mathbf{A}(\mathbf{t})\mathbf{x}(\mathbf{t}) + \mathbf{B}(\mathbf{t})\mathbf{u}(\mathbf{t}) \quad (38)$$

$$\mathbf{y}(\mathbf{t}) = \mathbf{C}(\mathbf{t})\mathbf{x}(\mathbf{t}) + \mathbf{D}(\mathbf{t})\mathbf{u}(\mathbf{t}) \quad (39)$$

The vector $\mathbf{x}(\mathbf{t})$ is known as the state vector, whose elements contained in it are the state variables, defined by [16] as the smallest set of linearly independent system variables that, together with the values of the variables at t_0 and the forcing functions, will determine the value for all system variables for all $t \geq t_0$. Furthermore, for a system of order n , there will be n equations of state, which will be first-order simultaneous differential equations, where the n variables to be solved are the state variables.

Regarding the other elements contained in Equations 38 and 39, $\dot{\mathbf{x}}(\mathbf{t})$ is the derivative of the state vector with respect to time, $\mathbf{A}(\mathbf{t})$ is the system matrix, $\mathbf{B}(\mathbf{t})$ is the input matrix, and $\mathbf{u}(\mathbf{t})$ is the input vector. Hence, $\mathbf{y}(\mathbf{t})$ is the output vector, \mathbf{C} the output matrix and $\mathbf{D}(\mathbf{t})$ is known as the feedforward matrix.

The state space approach can model and design various physical systems, such as mechanical or electrical circuits. This work will focus on modeling electrical circuits since this is how the CVS is represented. So, the modeling presented in this work follows the format shown in Equation 38, with $\dot{\mathbf{x}}(\mathbf{t}) = \mathbf{A}(\mathbf{t})\mathbf{x}(\mathbf{t}) + \mathbf{b}(\mathbf{t})$, where we have as state vector $\mathbf{x}(\mathbf{t}) = [V_{la}(t), V_{lv}(t), P_{ao}(t), Q_a(t), P_{as}(t), P_{vs}(t), V_{ra}(t), V_{rv}(t), Q_p(t), P_{ap}(t), P_{vp}(t)]^T$. The system matrix $\mathbf{A}(\mathbf{t})$ is formed by the coefficients of the state variables, while matrix $\mathbf{b}(\mathbf{t})$ is formed by the constants present in the state equations presented earlier.

In addition, a vector $x(t_0)$ containing the initial conditions of the state vector was used. Thus, a computational simulation of the system was performed using MATLAB[®] software, where the

initial state used was as follows:

$$x(t_0) = [68.0, 125.0, 80.0, 0.0, 72.0, 8.8, 20.0, 125.0, 12.0, 0.0, 10.0]^T$$

The technique used to solve this system was the fourth-order Runge-Kutta numerical integration method with an integration step of 0.0001. The parameters used for a healthy patient are shown in the table 2.2 and were based on that proposed by [11].

Table 2.2: Model Parameters.

<i>Parameter</i>	<i>Value</i>
<i>Resistances (mmHg · s/mL)</i>	
Mitral Valve Resistance (R_m)	0.003000
Aortic Valve Resistance (R_a)	0.007500
Systemic Characteristic Resistance (R_{cs})	0.049500
Systemic Arterial Resistance (R_{as})	0.790500
Systemic Venous Resistance (R_{vs})	0.060000
Tricuspid Valve Resistance (R_t)	0.005250
Pulmonary Valve Resistance (R_p)	0.002250
Pulmonary characteristic Resistance (R_{cp})	0.002250
Pulmonary Arterial Resistance (R_{ap})	0.075000
Pulmonary Venous Resistance (R_{vp})	0.000750
<i>Compliances (mL/mmHg)</i>	
Systemic Arterial Compliance (C_{as})	3.470000
Systemic Venous Compliance (C_{vs})	84.000000
Pulmonary Arterial Compliance (C_{ap})	4.000000
Pulmonary Venous Compliance (C_{vp})	5.000000
<i>Inertances (mmHg · s²/mL)</i>	
Systemic Inertance (L_s)	0.000073
Pulmonary Inertance (L_p)	0.000035
<i>Volume Constants (mL)</i>	
V_{lv_0} (mL)	5.000000
V_{rv_0} (mL)	20.000000
V_{la_0} (mL)	4.000000
V_{ra_0} (mL)	4.000000

In addition, all ideal diodes have their initial state set to 0, and the heart rate used to simulate a healthy patient was 72 bpm. Figures 13 and 14 show the results of this simulation. They show the left heart and the right heart results, respectively.

Figure 13 displays, in the first graph, the pressures in the aorta (P_{ao}), left ventricle (V_{lv}), and left atrium (V_{la}). The second graph is the flow in the aorta (Q_a), and the last one shows the volume in the left ventricle (V_{lv}) and left atrium (V_{la}).

Figure 13: Left Heart simulated curves.

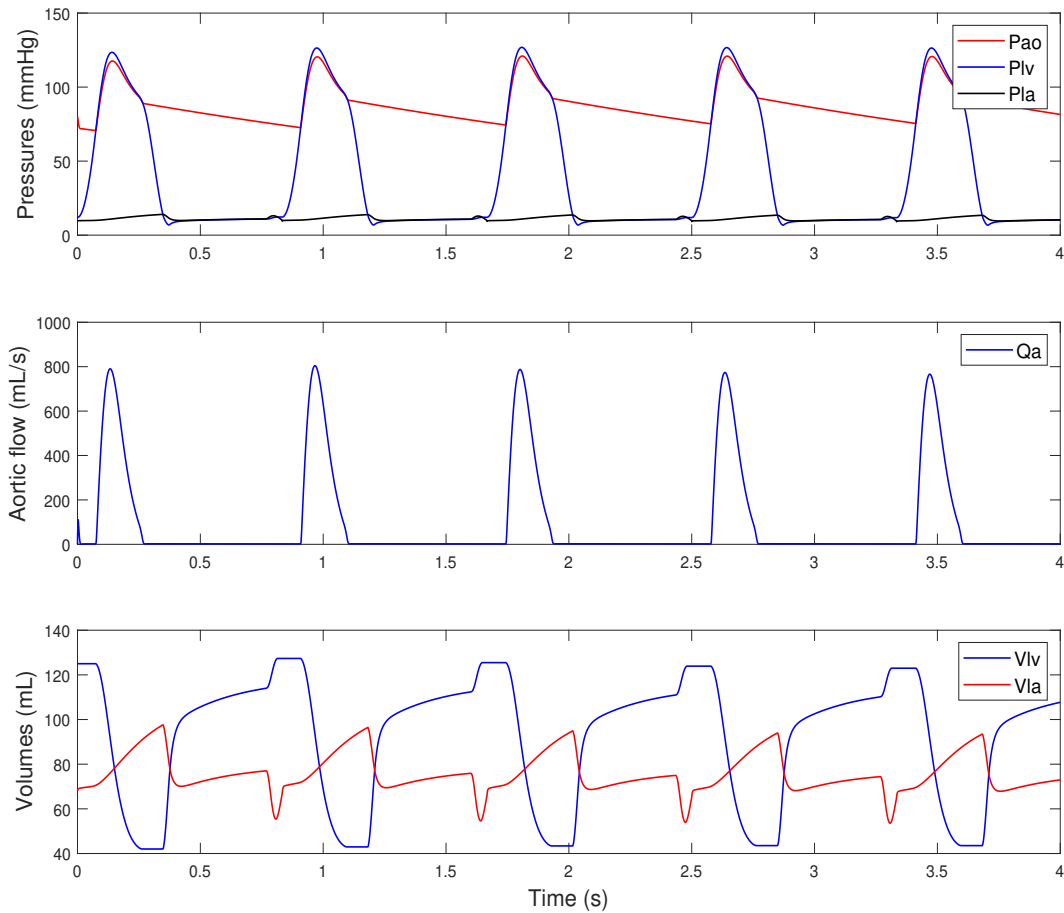
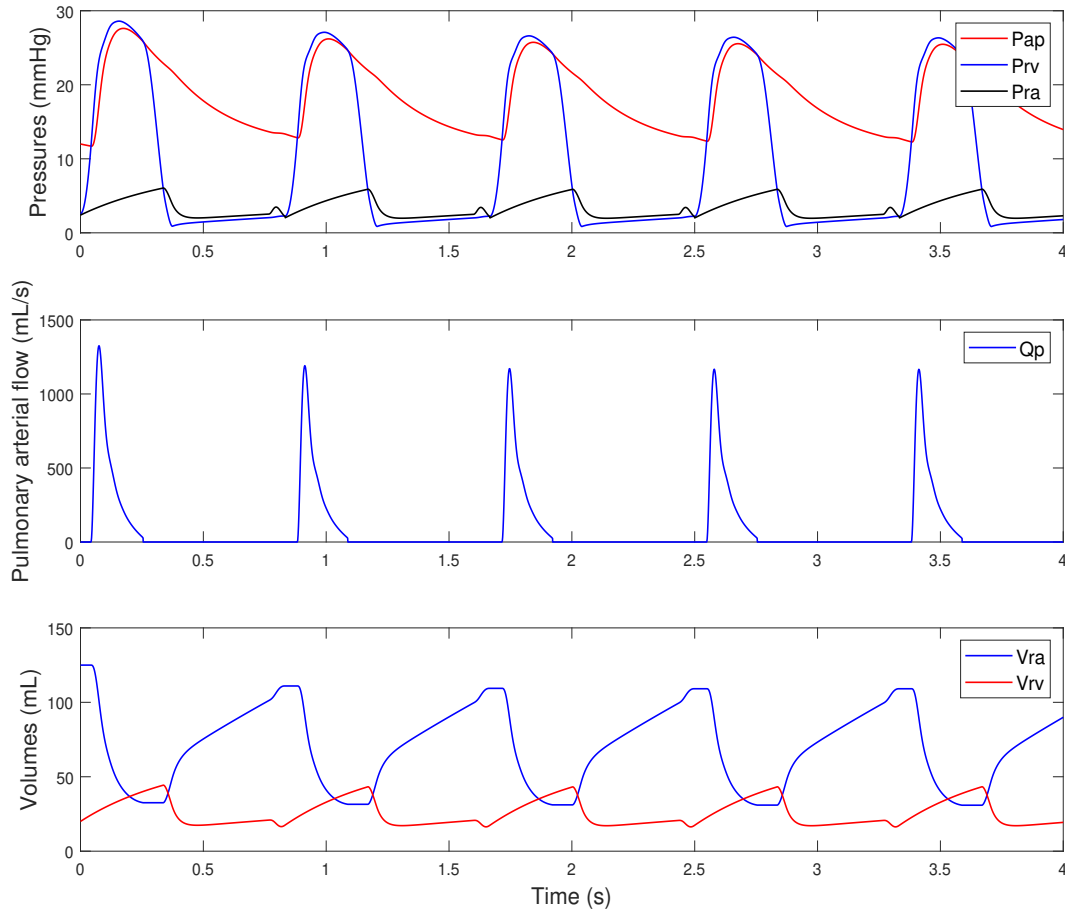


Figure 14 shows, in the first graph, the pressures in the pulmonary artery (P_{ap}), right ventricle (V_{rv}), and right atrium (V_{ra}). The second graph shows the pulmonary flow (Q_p), and the third graph shows the volumes in the right ventricle (V_{rv}) and right atrium (V_{ra}).

Figure 14: Right Heart simulated curves.



[2] explain that during diastole, the volume in the ventricles usually reaches about 110 to 120 mL. However, it also can reach 150 or 180 mL in a healthy heart when large amounts of blood reach the ventricles. This volume is called end-diastolic volume (EDV). During systole, this volume decreases by about 70 mL, this decrease is called stroke volume (SV), and the remaining volume, about 40 to 50 mL in systole, is called end-systolic volume (ESV). Thus, the stroke volume is the difference between the diastolic and systolic end volumes, according to Equation 40.

$$SV = EDV - ESV \quad (40)$$

The fraction of blood driven from the diastolic end volume is called the ejection fraction (EF) and is equivalent to about 60%. The calculation used for the ejection fraction was done according to Equation 41.

$$EF = \frac{SV}{EDV} \times 100 \quad (41)$$

[2] also define cardiac output (CO) as the amount of blood pumped by the heart that passes through the aorta per minute. It is the sum of blood flow to all tissues of the body. For a young,

healthy man at rest, the cardiac output stands at about 5.6 L/min, and for women, at about 4.9 L/min. With advancing age, there is a decrease in cardiac output value. For an adult, cardiac output is often defined as about 5 L/min. To calculate cardiac output, Equation 42 was used, which consists of multiplying the systolic output by the heart rate.

$$CO = HR \times SV \quad (42)$$

Finally, mean arterial pressure (MAP) is the average of the arterial pressures measured at time steps within one cardiac cycle. A mean arterial pressure between 70 and 100 mmHg is usually considered healthy.

Some metrics besides the visualization of the cardiac curves were applied to validate the CVS model and the parameters used in the computer simulation. Systolic and diastolic end volumes, stroke volume, mean arterial pressure, ejection fraction, and cardiac output were calculated for healthy heart rates. All these metrics were calculated for both heart sides according to the above mentioned techniques. These metrics results are displayed in the following Table 2.3.

Table 2.3: Simulated physiological measurements for a healthy patient at various heart rates.

Left Heart						
HR (bpm)	MAP (mmHg)	EDV (mL)	ESV (mL)	SV (mL)	EF (%)	CO (L/min)
60	79.2	130.5	41.4	89.1	68.26	5.34
72	83.5	121.9	43.2	78.6	64.53	5.66
80	85.9	117.3	44.3	73.0	62.21	5.84
Right Heart						
HR (bpm)	MAP (mmHg)	EDV (mL)	ESV (mL)	SV (mL)	EF (%)	CO (L/min)
60	79.2	120.6	31.5	89.1	73.80	5.34
72	83.5	109.5	30.8	78.6	71.82	5.66
80	85.9	103.4	30.4	73.0	70.56	5.84

The level of tension applied to the heart muscle at the beginning of the contraction is called preload—the greater this tension, the greater the pressure. The afterload is the resistance faced by the muscle when exerting the contractile force during ejection. According to [8], another way to validate the model is to vary the preload and afterload conditions of the model while keeping the other parameters constant (E_{max} , E_{min} , V_0). Doing so makes it possible to obtain an approximately linear relationship between end-systolic volume and end-systolic pressure. This relationship is known as the End-Systolic Pressure-Volume Relationship (ESPVR).

To reproduce these conditions of varying preload and afterload, it is necessary to vary mitral resistance (R_m) in the preload case and systemic arterial resistance (R_{as}) in the afterload case. In

each case, different values were selected for each resistor, and the results are shown in Figures 15(a) and 15(b).

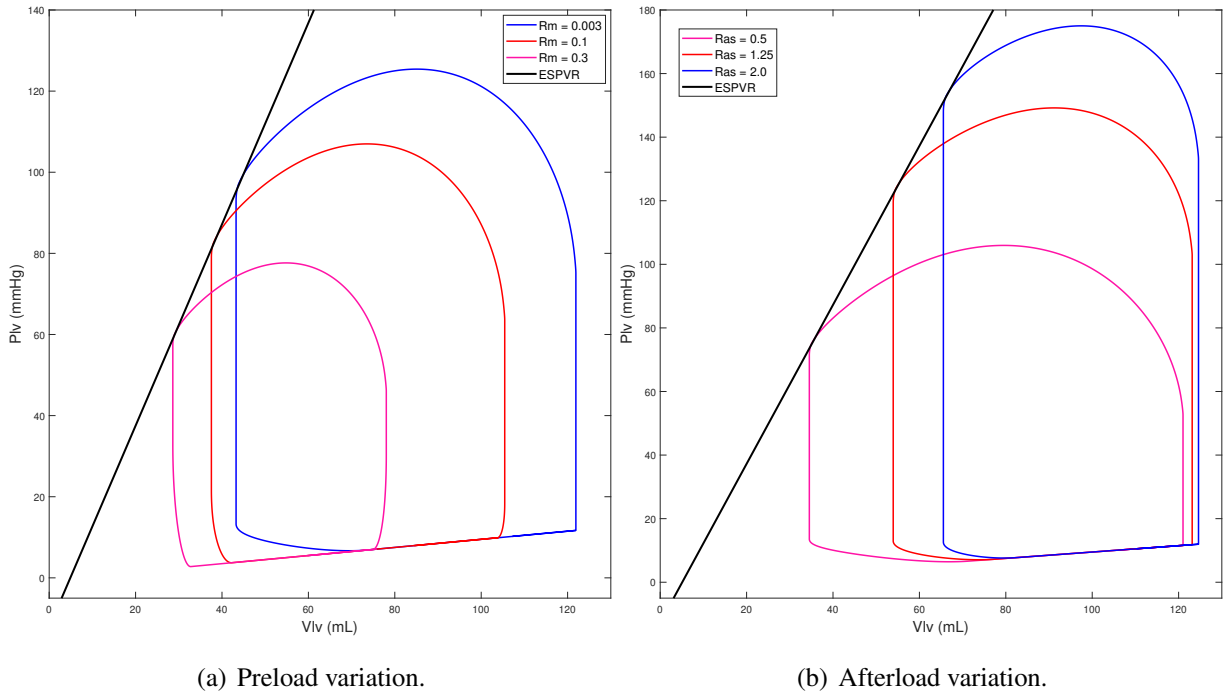


Figure 15(a) shows the behavior of the pressure-volume diagram with changing preload conditions in the left ventricle. For this purpose, three different values for R_m were selected, as shown in the figure legend. The ESPVR curve behaved linearly, as expected. Furthermore, the straight line has a slope of 2.48, which is approximately the value of $E_{lv,max}$ and crosses the horizontal axis at $V_{lv}(t) \approx 4.89$ mL, which is close to the value of $V_{lv,0}$ which is 5.0 mL.

Figure 15(b) also shows the pressure-volume diagram, but with changes in the afterload conditions. These changes were made by selecting three different values for R_{as} . The ESPVR straight line also shows the same linear behavior, it has a slope of 2.5, and crosses the horizontal axis at approximately 5.1 mL.

2.3 Final Considerations

This chapter introduced the cardiac anatomy, main variables, and states involved in the cardiac cycle. The chosen modeling of the cardiovascular system was 0D modeling, based on first-order ordinary differential equations. For this reason, a brief comment was made on modeling linear time-invariant systems. Although this is not the system classification present in this work, comments serve as an introduction to the subject. With the simulation of this system concluded

and the values of the hemodynamic variables validated, coupling a VAD model for performance studies and developing control techniques through simulation is possible. This issue will be addressed in the following chapters. The source code of this chapter's simulations can be accessed on the link <https://github.com/Roger987/A-framework-of-the-Human-Cardiovascular-System/tree/main/Model%20DiMolfetta%202010%20-%20with%20Cao>.

3

Ventricular Assist Devices

This chapter aims to introduce the concept of VADs through some data and definitions and explain the different types of available devices. Then, a model of a continuous flow LVAD coupled to the cardiovascular system is presented, and its equations are deduced, as done with the CVS model in the previous chapter. Finally, the results of a computer simulation of this model are shown.

3.1 Ventricular Assist Devices

Ventricular assist devices are mechanical circulatory support devices developed as a treatment strategy for patients with end-stage heart failure. They can be used to support failing left and right ventricles. They were initially conceived as temporary bridge-to-transplant (BTT) platforms while patients waited until a donor organ became available.

However, other usages of these devices were found over time. Destination therapy (DT) with VADs has become potentially a durable, even lifelong, alternative to HT. From January 2010 to December 2019, 25,551 continuous flow (CF) LVADs were implanted in the US. Of these implantations, 50.4% were for DT, and 21.9% were for BTT. The remaining 27.7% includes bridge-to-candidacy (BTC), bridge-to-decision (BTD), and bridge-to-recovery (BTR) [17, 18, 19].

According to the society of thoracic surgeons in the 2020 Annual Intermacs Report, 3,198 left ventricular assist devices (LVADs) were implemented in 2019 in the US. This number was the highest annual volume in their history, showing a growing demand for these devices. Patients with these therapies had a 1-year and 2-year survival of 82.3% and 73.1%, respectively, between 2015 and 2019. They also had some adverse effects, with major bleeding and infection being the most recurrent ones [17].

Over the years, some different types of VADs have been developed. Because of that, they are usually divided into generations. The first generation tried to reproduce the pulsatility of the

native heart. They are known as volume displacement devices, being pneumatically driven and pulsatile flow. They were unreliable, having a high risk of infection, thrombus formation, and blood trauma, which implies poor survival. These pulsatile pumps are produced by companies such as Thoratec[®] or Berlin Heart[®] [18, 19]. Despite the limitations, these first-generation pumps have significantly decreased deaths related to HF. The 1-year survival with only medical therapy was 25% versus 52% with LVAD treatment [20].

Figure 15: Thoratec's Heartmate I[®] (left) and Heartmate II[®] (right).

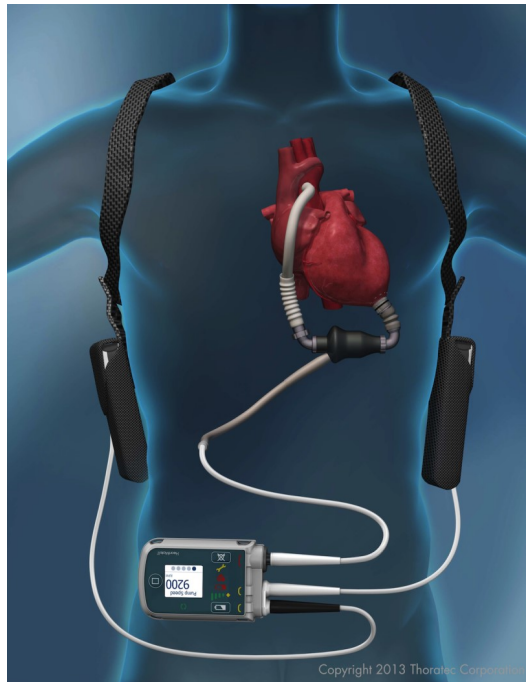


Copyright 2006 Thoratec Corporation

Note. Comparison between heartmate I and heartmate II. From *The past, present and future of the device keeping alive Carew, thousands of HF patients*, by American Heart Association, 2018, (<https://www.heart.org/en/news/2018/06/13/the-past-present-and-future-of-the-device-keeping-alive-carew-thousands-of-hf-patients>). Copyright 2006 Thoratec Corporation.

The second-generation LVADs tried to improve the first-generation limitations by being smaller and more durable and expanding their potential as a mainstream therapy for HF. The continuous flow devices are characterized by producing a continuous flow via a rotating impeller inside a small pump chamber. These pumps can have axial, centrifugal, or mixed flow mechanisms. The axial flow is generated with a propeller in a pipe. On the other hand, the centrifugal flow is generated with a bladed disk spinning in a cavity. Despite some concerns about whether a 'non-pulsatile' blood flow could support long-term end-organ function, numbers have shown significant improvement in survival for both DT and BTT patients [18].

Figure 16: Heartmate II.



Note. Heartmate II[®] coupled to a human heart. From *The past, present and future of the device keeping alive Carew, thousands of HF patients*, by American Heart Association, 2018, (<https://www.heart.org/en/news/2018/06/13/the-past-present-and-future-of-the-device-keeping-alive-carew-thousands-of-hf-patients>). Copyright 2013 Thoratec Corporation.

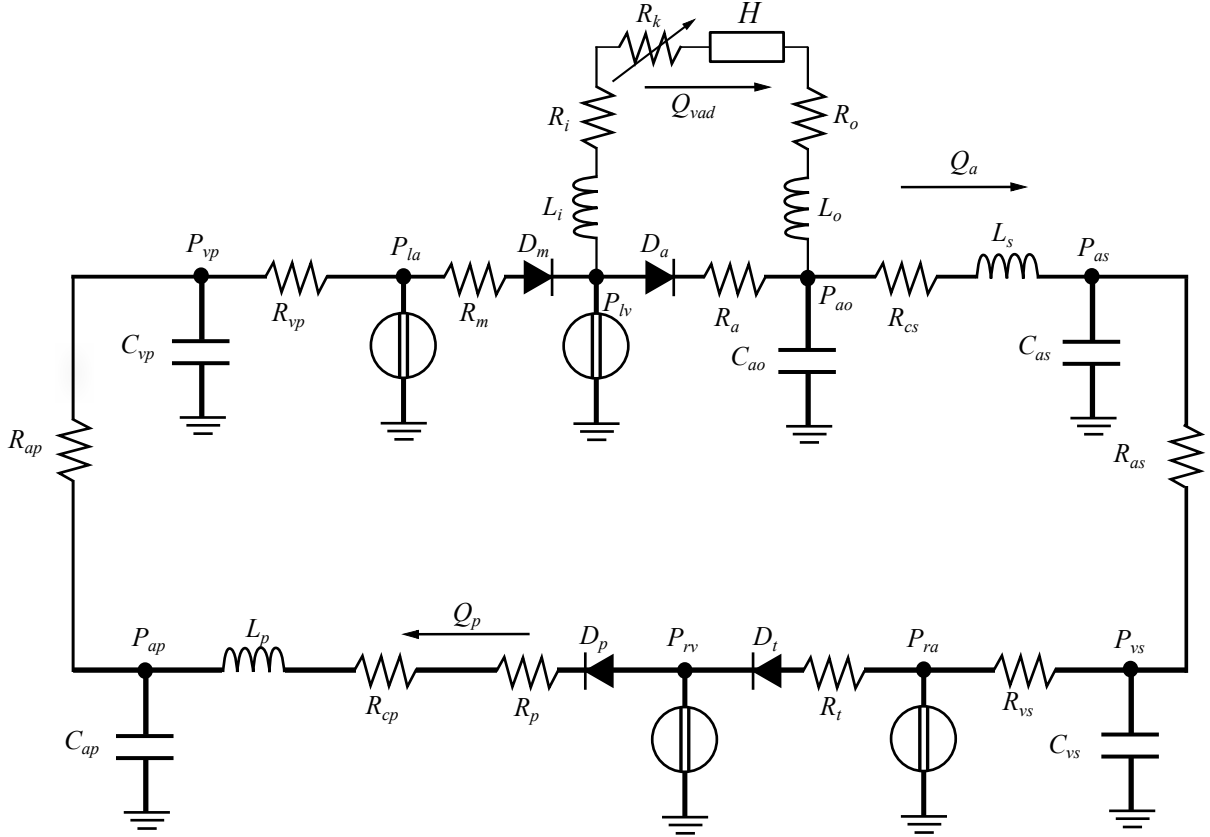
Figure 16 shows how Thoratec’s Heartmate II, a second-generation device, is implanted into the human body. An inlet cannula is coupled to the left ventricle, while an outlet cannula is attached to the aorta. A driveline exits at the level of the abdomen and is connected to an external power source that powers the impeller blade. These second-generation LVADs can provide rotatory speeds between 8,000 and 15,000 rpm [20].

Finally, the third generation of LVADs uses a fully magnetically levitated impeller, with a technology known as MAGLEV – Magnetic Levitation. It allows these devices to have rotation without friction or wear. This non-contact bearing is the main difference between second and third-generation devices. Besides that, they also have wider blood-flow paths and artificial pulsatility [19][20].

3.2 The LVAD Model

This work uses the axial flow pump model proposed by [21]. Figure 17 shows the electric circuit analogous to the CVS system with the addition of the pump model. The pump is connected as a bridge between the left ventricle and the aorta, as shown in Figure 16, and as done by [8].

Figure 17: LVAD model attached to the cardiovascular model.



Consequently, the pump's addition to the system has added a new state variable, so the CVS+LVAD model is a twelfth-order system. This new state variable, Q_{vad} , represents the pump's flow, and five new passive elements are added to the model. R_i and R_o represent the inlet and outlet resistances of the pump cannulae. L_i e L_o represents the inlet and outlet inertances of the pump cannulae. Finally, R_k is a time-varying and non-linear resistor reproducing the suction phenomenon and is given by Equation 43.

$$R_k = \begin{cases} \alpha(P_{lv}(t) - \bar{x}_1), & P_{lv}(t) \leq \bar{x}_1 \\ 0, & \text{otherwise.} \end{cases} \quad (43)$$

where alpha is an LVAD-dependent weight and \bar{x}_1 is a threshold pressure, their values are - 3.5 s/mL and 1 mmHg, respectively. Furthermore, the H in Figure 17 represents the pressure difference across the pump and is given by

$$H = \beta_0 Q_{vad} + \beta_1 \frac{dQ_{vad}}{dt} + \beta_2 \omega^2 \quad (44)$$

where ω is the pump speed, Q_{vad} is the pump flow, and β_0 , β_1 and β_2 are LVAD-dependent parameters. The values of these parameters are shown in table 3.1.

Finally, as done before with the cardiovascular model, basic circuit analysis was applied

to the model with the pump to find its analytical representation. Since this is a twelfth-order system, twelve first-degree differential equations were deduced using Kirchhoff's laws. These equations are shown below:

- **Left Atrial Volume** ($\dot{V}_{la}(t)$)

$$\begin{aligned} \dot{V}_{la}(t) = & - \left[\frac{1}{R_{vp}} + \frac{D_m}{R_m} \right] E_{la}(t)V_{la}(t) + \frac{D_m}{R_m} E_{lv}(t)V_{lv}(t) + \frac{P_{vp}(t)}{R_{vp}} \\ & + \left[\frac{1}{R_{vp}} + \frac{D_m}{R_m} \right] E_{la}(t)V_{la0} - \frac{D_m}{R_m} E_{lv}(t)V_{lv0} \end{aligned} \quad (45)$$

- **Left Ventricular Volume** ($\dot{V}_{lv}(t)$)

$$\begin{aligned} \dot{V}_{lv}(t) = & \frac{D_m}{R_m} E_{la}(t)V_{la}(t) - \left[\frac{D_m}{R_m} + \frac{D_a}{R_a} \right] E_{lv}(t)V_{lv}(t) - Q_{vad}(t) \\ & - \frac{D_m}{R_m} E_{la}(t)V_{la0} + \left[\frac{D_m}{R_m} + \frac{D_a}{R_a} \right] E_{lv}(t)V_{lv0} + \frac{D_a}{R_a} P_{ao}(t) \end{aligned} \quad (46)$$

- **VAD Flow** ($\dot{Q}_{vad}(t)$)

$$\dot{Q}_{vad}(t) = \frac{E_{lv}(t)V_{lv}(t)}{L^*} - \frac{R^*}{L^*} Q_{vad}(t) - \frac{P_{ao}(t)}{L^*} - \frac{\beta_2 \omega^2}{L^*} - \frac{E_{lv}(t)V_{lv0}}{L^*} \quad (47)$$

- **Aortic Pressure** ($\dot{P}_{ao}(t)$)

$$\begin{aligned} \dot{P}_{ao}(t) = & \frac{D_a}{R_a C_{ao}} E_{lv}(t)V_{lv}(t) + \frac{1}{C_{ao}} Q_{vad}(t) - \frac{D_a}{R_a C_{ao}} P_{ao}(t) \\ & - \frac{1}{C_{ao}} Q_a(t) - \frac{D_a}{R_a C_{ao}} E_{lv}(t)V_{lv,0} \end{aligned} \quad (48)$$

- **Arterial Flow** ($\dot{Q}_a(t)$)

$$\dot{Q}_a(t) = -\frac{R_{cs}}{L_s} Q_a(t) - \frac{P_{as}(t)}{L_s} + \frac{P_{ao}(t)}{L_s} \quad (49)$$

- **Systemic Pressure** ($\dot{P}_{as}(t)$)

$$\dot{P}_{as}(t) = \frac{Q_a(t)}{C_{as}} - \frac{P_{as}(t)}{R_{as} C_{as}} + \frac{P_{vs}(t)}{R_{as} C_{as}} \quad (50)$$

- **Systemic Venous Pressure** ($\dot{P}_{vs}(t)$)

$$\dot{P}_{vs}(t) = \frac{P_{as}(t)}{R_{as}C_{vs}} - \left[\frac{1}{R_{as}} + \frac{1}{R_{vs}} \right] \frac{P_{vs}(t)}{C_{vs}} + \frac{E_{ra}(t)V_{ra}(t)}{R_{vs}C_{vs}} - \frac{E_{ra}(t)V_{ra0}}{R_{vs}C_{vs}} \quad (51)$$

- **Right Atrial Volume** ($\dot{V}_{ra}(t)$)

$$\begin{aligned} \dot{V}_{ra}(t) = & - \left[\frac{1}{R_{vs}} + \frac{D_t}{R_t} \right] E_{ra}(t)V_{ra}(t) + \frac{D_t}{R_t} E_{rv}(t)V_{rv}(t) + \frac{P_{vs}(t)}{R_{vs}} \\ & + \left[\frac{1}{R_{vs}} + \frac{D_t}{R_t} \right] E_{ra}(t)V_{ra0} - \frac{D_t}{R_t} E_{rv}(t)V_{rv0}(t) \end{aligned} \quad (52)$$

- **Right Ventricular Volume** ($\dot{V}_{rv}(t)$)

$$\dot{V}_{rv}(t) = \frac{D_t}{R_t} E_{ra}(t)V_{ra}(t) - \frac{D_t}{R_t} E_{rv}(t)V_{rv}(t) - Q_p(t) + \frac{D_t}{R_t} (E_{rv}(t)V_{rv0} - E_{ra}(t)V_{ra0}) \quad (53)$$

- **Pulmonary Flow** ($\dot{Q}_p(t)$)

$$\dot{Q}_p(t) = -\frac{P_{ap}(t)}{L_p} - \left[\frac{R_p + R_{cp}}{L_p} \right] Q_p(t) + \frac{E_{rv}(t)V_{rv}(t)}{L_p} - \frac{E_{rv}(t)V_{rv0}}{L_p} \quad (54)$$

- **Pulmonary Pressure** ($\dot{P}_{ap}(t)$)

$$\dot{P}_{ap} = -\frac{P_{ap}}{R_{ap}C_{ap}} + \frac{Q_p}{C_{ap}} + \frac{P_{vp}}{R_{ap}C_{ap}} \quad (55)$$

- **Pulmonary Venous Pressure** ($\dot{P}_{vp}(t)$)

$$\dot{P}_{vp}(t) = \frac{E_{la}(t)V_{la}(t)}{R_{vp}C_{vp}} + \frac{P_{ap}(t)}{R_{ap}C_{vp}} - \left[\frac{1}{R_{ap}} + \frac{1}{R_{vp}} \right] \frac{P_{vp}(t)}{C_{vp}} - \frac{E_{la}(t)V_{la0}}{R_{vp}C_{vp}} \quad (56)$$

In Equation 47, $L^* = L_i + L_o$ and $R^* = R_i + R_o + R_k$.

3.3 LVAD+CVS model simulation and validation

Finally, a computer simulation of the LVAD model coupled to the CVS model was performed with MATLAB[®] by using the previous equations. The additional parameters to this simulation are shown in Table 3.1.

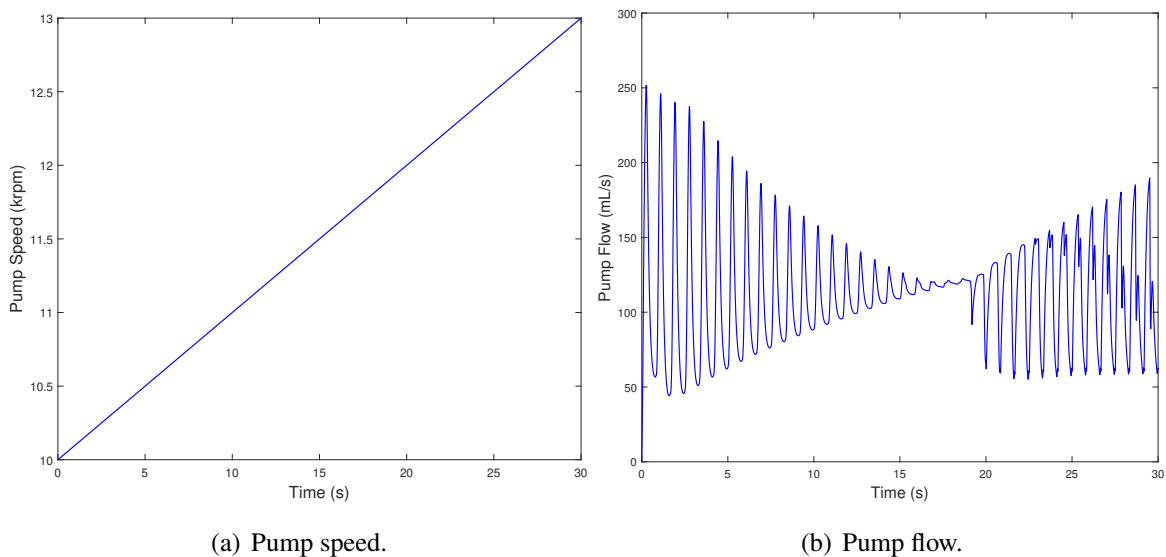
Table 3.1: Parameters of the LVAD model.

<i>Parameter</i>	<i>Value</i>
<i>Resistances (mmHg · s/mL)</i>	
Inlet Resistance of Cannulae (R_i)	0.0677
Outlet Resistance of Cannulae (R_o)	0.0677
Suction Resistance (R_k)	eq. 43
<i>Inertances (mmHg · s²/mL)</i>	
Inlet Inertance of Cannulae (L_i)	0.0127
Outlet Inertance of Cannulae (L_o)	0.0127
<i>Pressure Difference Parameters</i>	
β_0	0.17070
β_1	0.02177
β_2	-0.000093

In order to validate the model, it was necessary to study the behavior of the new state variable. So the pump speed in the simulation was linearly increased from an initial speed of 10,000 rpm to a final speed of 13,000 rpm over 30 seconds.

Figures 18(a) and 18(b) show, respectively, the pump speed linearly increasing during the time and the pump flow behavior during this same time. This behavior is similar to the one presented by [8]. In this case, the onset suction occurs approximately when the pump speed reaches 11,800 rpm, which is a phenomenon caused when the pump attempt to draw more blood than available because the speed is too high.

Figure 18: Pump speed linearly increasing and its respective behavior.

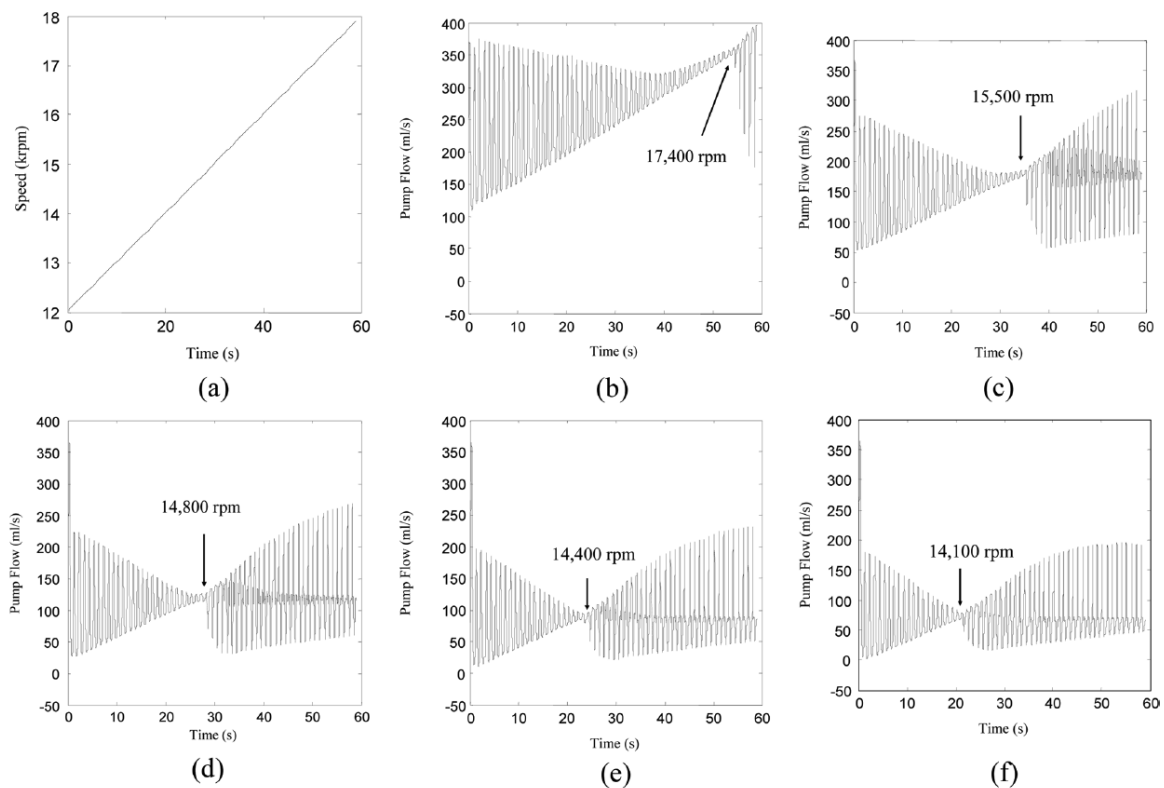


(a) Pump speed.

(b) Pump flow.

Figure 19 was extracted from the work of [8], and it shows some results of their simulations. Figure 19(a) shows the pump speed linearly increasing, and Figures 19(b)-(f) show the pump flow for different values of Systemic Vascular Resistance (SVR). Varying R_{as} can achieve these changes in the flow. It is possible to observe that onset suction occurs at a different point for each condition. Besides that, the general shape of these figures matches the shape of Figure 18(b) obtained in this work.

Figure 19: Pump speed (a) and pump flow for different values of SVR (b)-(f).



Note. Reprinted from *A Dynamical State Space Representation and Performance Analysis of a Feedback-Controlled Rotary Left Ventricular Assist Device*, by M. A. Simaan *et al.*, 2009, *IEEE Transactions on Control Systems Technology*, Volume 17.

3.4 Final Considerations

This chapter introduced the concept of ventricular assist devices and explained the different generations and types of available devices. It also showed some data concerning using LVADs as a bridge to transplant or destination therapy. Furthermore, it brought a numerical model of a second-generation LVAD and showed the results of a computer simulation of this numerical model. Finally, this computer simulation was validated by comparing the obtained results with the original paper's results.



An Immediate Response Starling-Like Controller

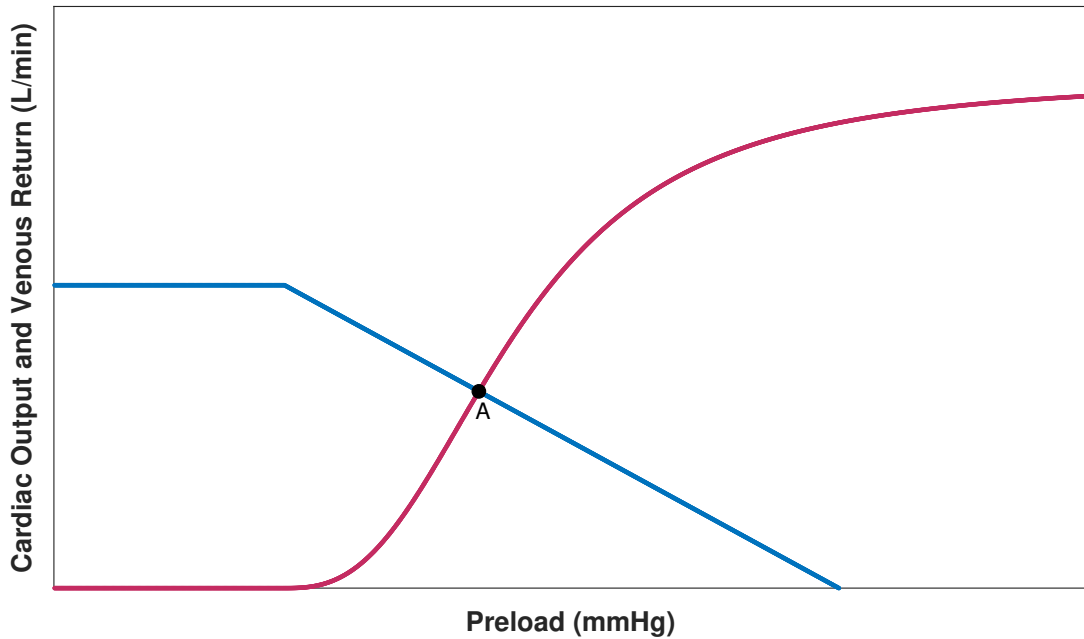
This chapter will introduce some control systems concepts and their applications in the context of left ventricular assist devices. Firstly, it will approach the Starling-like controller, a mechanism of control that aims to reproduce Starling's law behavior of the native heart to the pump. Then, this control technique will be applied to the CVS + LVAD model presented in the previous chapter. Other control techniques will also be addressed, such as proportional-integral control. Finally, simulation results will be presented.

4.1 Starling-Like Control

A way to express Starling's law is as a non-linear relationship between cardiac output and ventricular preload. The curves generated by this relation are defined as the cardiac response curves (CRCs). On the other hand, the normal venous return curve is a way to quantitatively represent the venous flow of blood into the heart from systemic circulation at different preload levels [2].

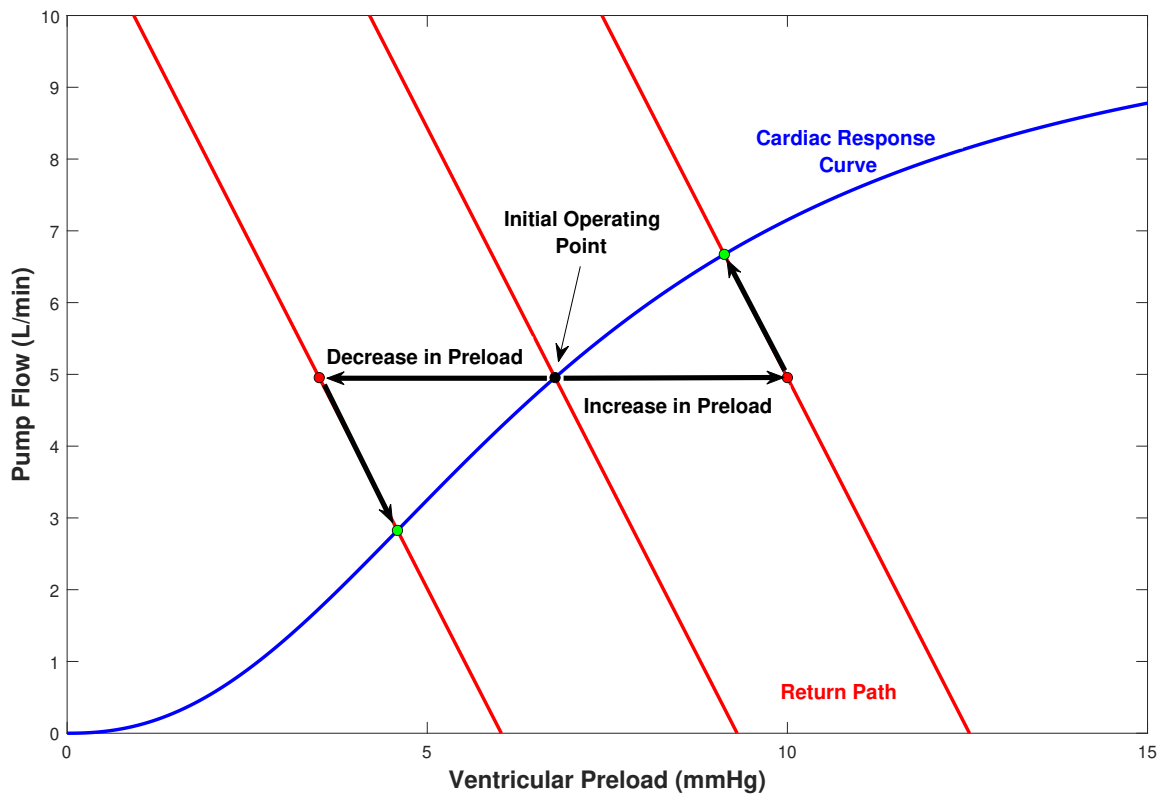
Finally, Guyton demonstrated that the venous return from the systemic circulation must be equal to the cardiac output from the heart with the same preload conditions [22]. Figure 20 shows both the venous return curve, in blue, and cardiac output, in red, with the preload being the x-axis. Point A is the equilibrium point, where the venous return curve equals the cardiac output with the same preload. In normal conditions, this point determines the cardiac output, the venous return, and preload.

Figure 20: Starling's Law.



Ventricular Assist Devices usually operate at a constant speed control (CSC), and this technique is not very sensitive to changes in the preload. Consequently, VADs cannot respond physiologically to the changes in the patient's cardiac demands, sometimes causing left ventricular suction and venous congestion [23][24].

Figure 21: Operating point trajectory on changing preload conditions.



A Starling-Like Controller (SLC) is a physiological technique of control that emulates Starling's Law from the native heart, and it is more able to respond to the changes in the preload. In this application, based on the work of [24], the left-ventricular end-diastolic pressure (P_{lved}) is used as a preload indicator; the pump flow is defined as the cardiac response curve, also known as the control line (CL), and a non-vertical linear return path emulates the venous return.

Figure 21 shows an initial operating point in the intersection between the control line, in blue, and the return path of this point, in red. The figure shows how the mechanism deals with changes in the preload, affecting this initial point's position. Increasing or decreasing the preload will result in a new return path, and the intersection of the control line with this new return path will be the new desired pump flow, represented by the green points.

The control line is given by a sigmoid function, as proposed by [24]. It is shown in Equation 57, where $\overline{Q_{vad}}$ represents the desired pump flow for each left-ventricular end-diastolic pressure. SF is a scaling factor used to adjust the preload sensitivity of the control line to attend to the patient's circulation demands. This scaling factor is fixed for immediate SLC, contrary to the adaptative SLC, which this work will not explore.

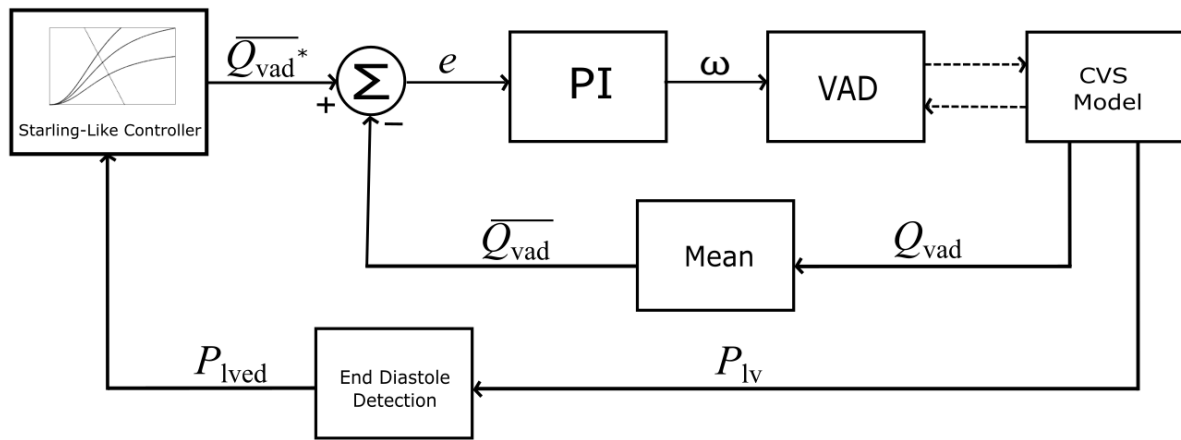
$$\overline{Q_{vad}}^* = \left[10.3 + \left(\frac{-10.3}{1 + \left(\frac{P_{lved}(t)}{7} \right)^{2.3}} \right) \right] \cdot SF \quad (57)$$

The return path is given by a simple linear equation, as shown in Equation 58, where $y(t)$ represents the return path, $x(t)$ represents the P_{lved} , x_1 represents the current P_{lved} and y_1 represents the current $\overline{Q_{vad}}$. The slope m of the line is -1.96 L/min/mmHg, the same used in [24].

$$y(t) = m(x(t) - x_1) + y_1 \quad (58)$$

Finally, Figure 22 shows the block diagram of the control system. A proportional-integral controller is used to minimize the error between $\overline{Q_{vad}}^*$ and $\overline{Q_{vad}}$, where $\overline{Q_{vad}}$ is measured mean pump flow. It receives the error signal as input and returns the LVAD speed as output, which affects the flow, reducing the difference between the target flow and the measured one.

Figure 22: Block Diagram of the physiological control system.



According to Stephens *et al.*, a limitation of the immediate Starling-like control is that a single CL appropriate for rest will not be appropriate for some changes in the circulatory state of the patient, such as exercise conditions [24]. However, it will be enough for the objectives of this work.

4.2 Controller Simulation and Validation

Once again, the simulations of the system controlled by the control techniques presented in this chapter were performed using MATLAB[®]. The Starling-like control was implemented considering the mean of the target flow as the intersection between Equations 57 and 58. This value is the input signal to the proportional-integral controller. On the other hand, \overline{Q}_{vad} is the mean of the measured flow of the CVS model of each cardiac cycle, and it is the controller's feedback. Finally, the controller's output is the VAD speed $\omega(t)$.

Equation 59 is the PI controller's equation, where the gains were obtained empirically. The values of K_p and K_i are, respectively, 40 and 75, and $e(t)$ is the error signal, which is the difference between \overline{Q}_{vad} and \overline{Q}_{vad}^* .

$$\omega(t) = K_p \cdot e(t) + K_i \int_0^t e(\tau) d\tau \quad (59)$$

In order to simulate a heart failure patient, the maximum left-ventricular elastance was decreased from 2.5 mmHg/mL to 1.2 mmHg/mL.

Finally, two tests were performed in order to validate the Starling-like controller. The first increased the left-ventricular end-diastolic pressure, and the second decreased the pressure.

In the first test, the mitral valve resistance was changed from 0.003 to 0.05 mmHg · s/mL at 12 seconds, causing an increase in P_{lved} . Figure 23 shows both the R_m values and P_{lved}

through time. On the other hand, Figure 24 shows measured flow in comparison to the target flow through time, and Figure 25 shows the pump speed and the pump flow. Finally, Figure 26 shows the trajectory of the operating point into the cardiac response curve, showing that the controller is working as it should.

Figure 23: Left-ventricular end-diastolic pressure and the resistance of the mitral valve through time with the increase of P_{lved} at 12 seconds.

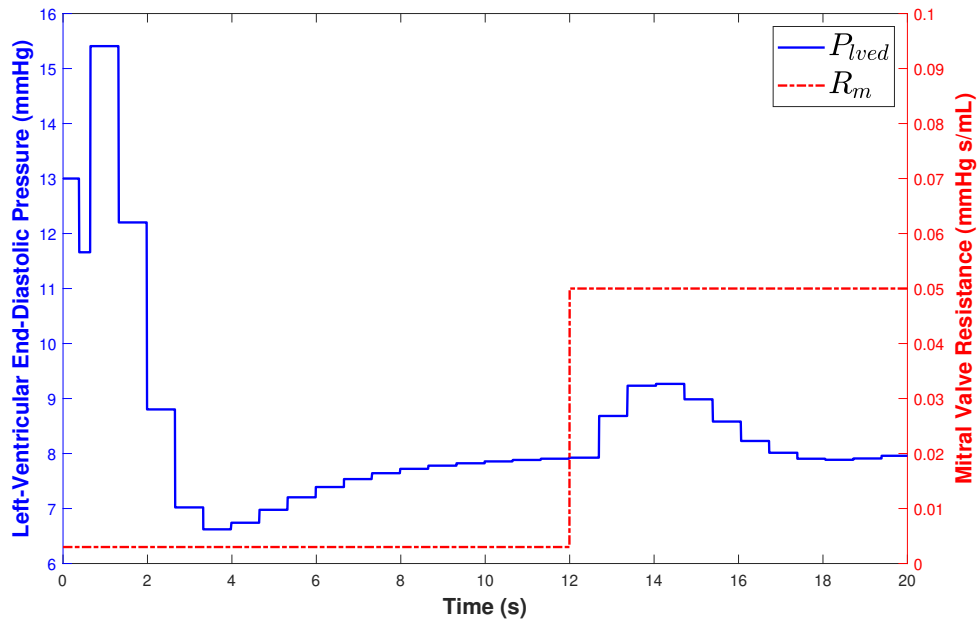


Figure 24: Mean measured flow and mean target flow comparison through time, showing how the controller worked after increase P_{lved} at 12 seconds.

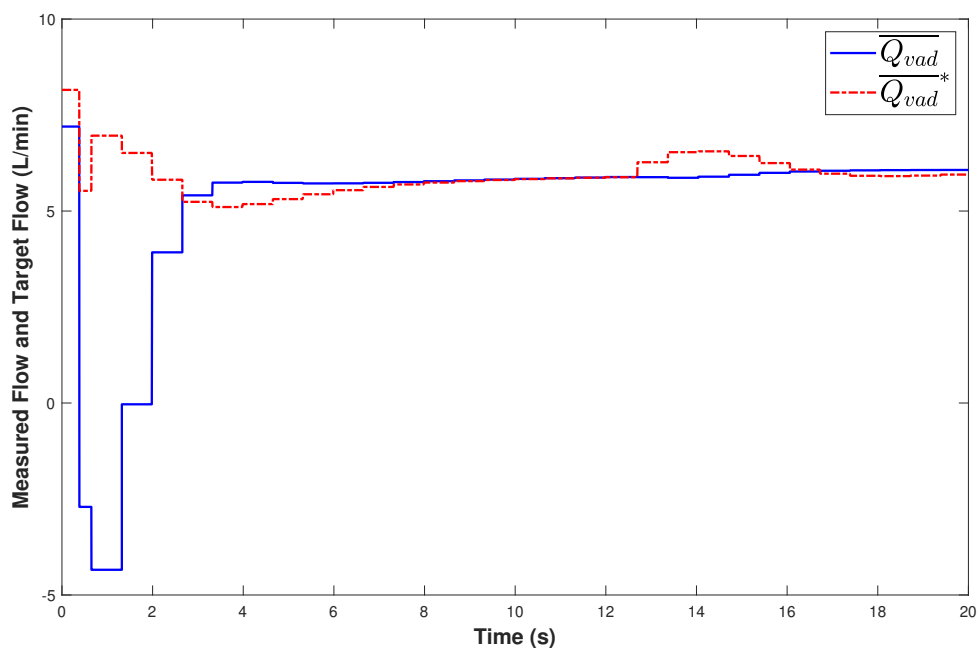


Figure 25: Pump flow and pump speed vary according to the controller. The speed increases with the increase of P_{lved} .

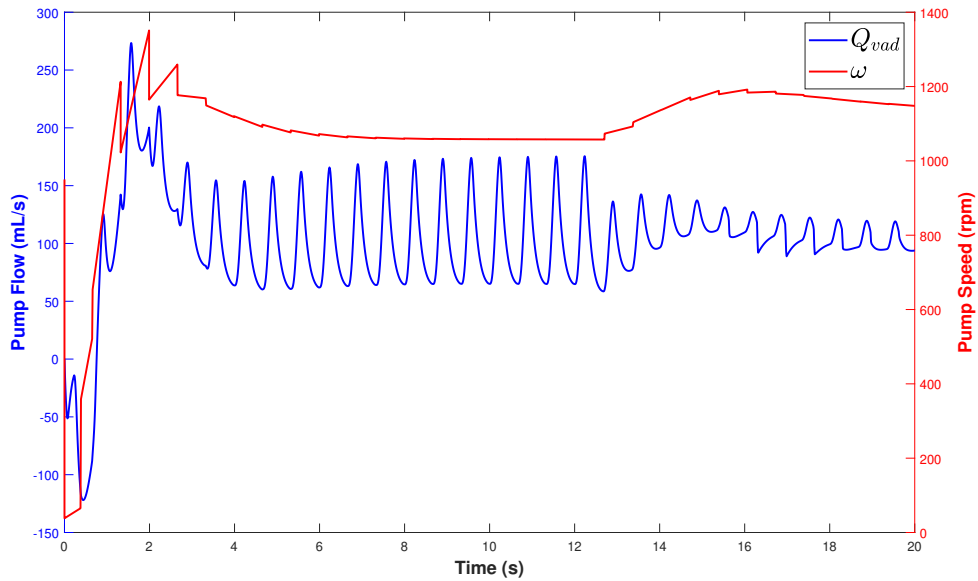
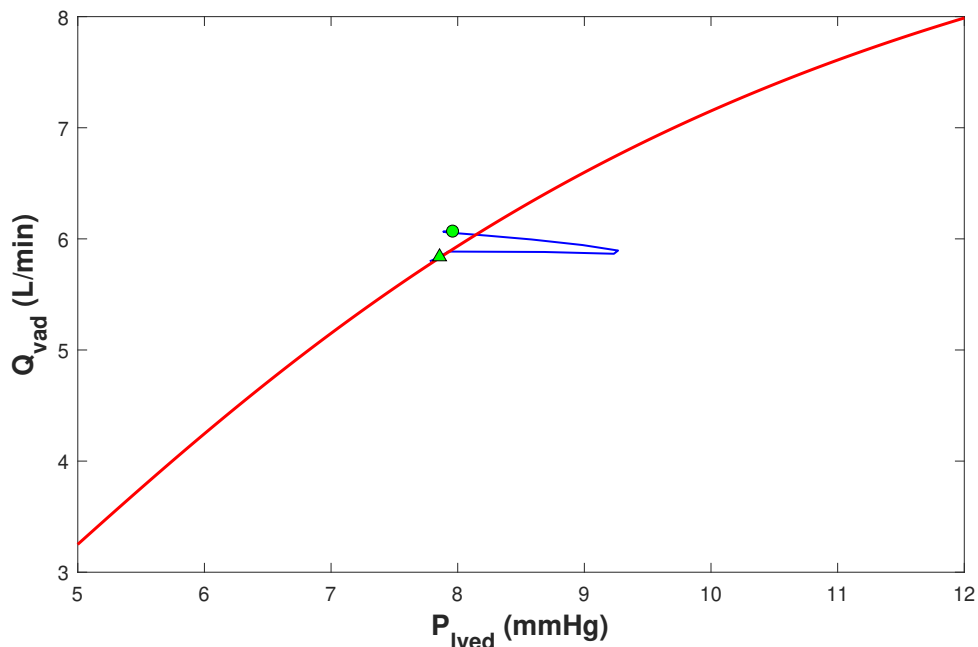


Figure 26: Operating point trajectory. Before the disturbance, it is located on the triangle point. Then, the increase in the preload conditions pulls it to the right side of the CL, and the controller brings it back to the CL (on the circle point).



The second test consisted of changing the mitral valve resistance from 0.003 to 0.01 $mmHg \cdot s/mL$ at 12 seconds, causing a decrease in P_{lved} . Figure 23 shows both the R_m values and P_{lved} through time, where the pressure value is reduced after 12 seconds, and it is adjusted by the controller at a time of approximately 15 seconds. Figure 28 shows the measured flow in comparison to the target flow, where a disturbance can also be spotted at 12 seconds, and both

curves converge at 15 seconds. Figure 29 shows the pump speed and the pump flow. Finally, Figure 30 shows the trajectory of the operating point into the cardiac response curve.

Figure 27: Left-ventricular end-diastolic pressure and the resistance of the mitral valve through time with the decrease of P_{lved} at 12 seconds.

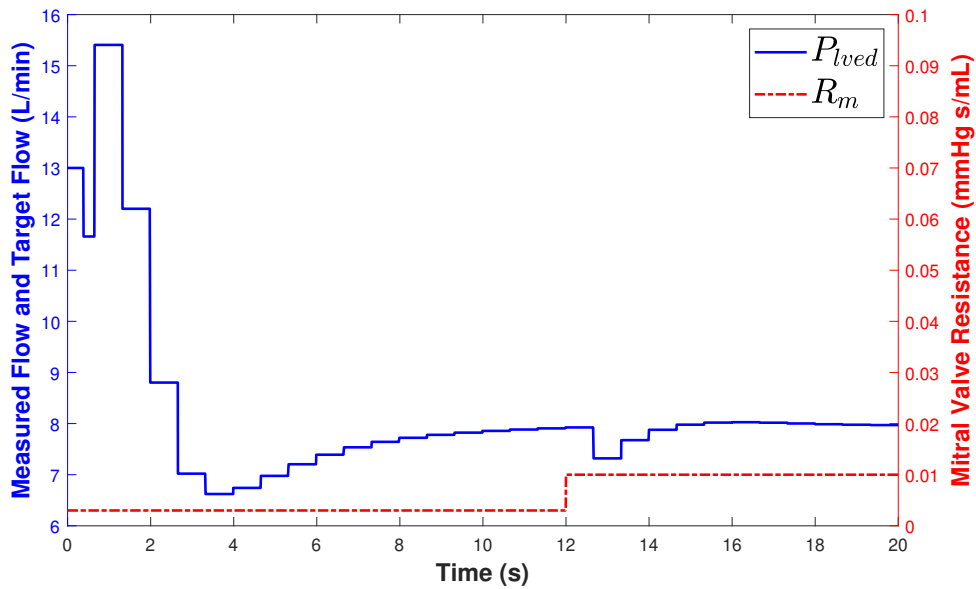


Figure 28: Mean measured flow and mean target flow comparison through time, showing how the controller worked after decrease P_{lved} at 12 seconds.

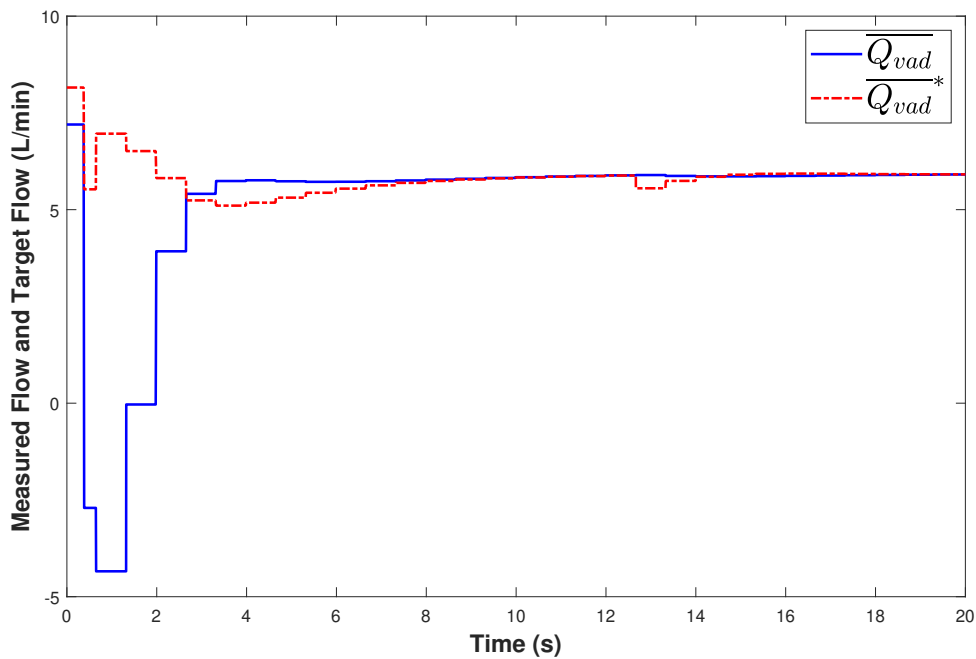


Figure 29: Pump flow and pump speed vary according to the controller. The speed decreases with the decrease of P_{lved} .

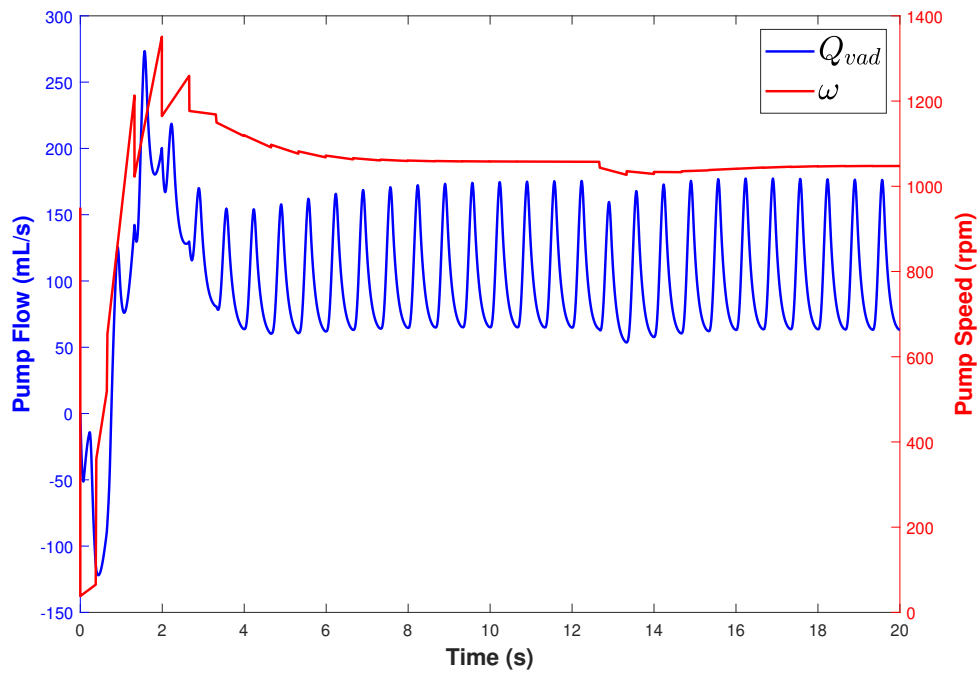
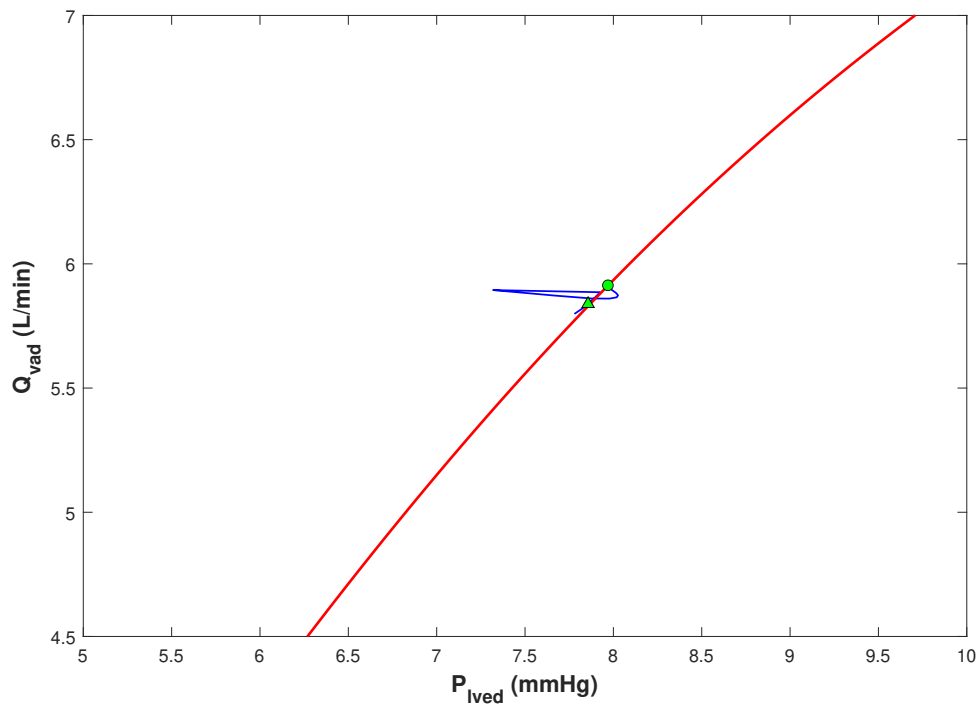


Figure 30: Operating point trajectory. Its initial position is the triangle point. Then, the decrease in the preload conditions pulls it to the left side of the CL, and the controller brings it back to the CL (on the circle point).



4.3 Final Considerations

This chapter proved that it is possible to use the framework of the coupled model (CVS + LVAD) to control purposes. Although only a physiological control technique was studied and presented, other control strategies can be used in future research. Two tests were performed, and in both of them, the system was controlled successfully. The source code of this chapter's simulations can be accessed on the link <https://github.com/Roger987/A-framework-of-the-Human-Cardiovascular-System-/tree/main/Model%20with%20Starling-like%20control>. The entire project can be accessed on the link <https://github.com/Roger987/A-framework-of-the-Human-Cardiovascular-System->

5

Conclusion

This work has successfully developed a framework to simulate the behavior of the human cardiovascular system, considering both sides of the heart, based on numerical models from other works. Besides that, a continuous flow left ventricular assist device was coupled to this framework, and a control technique based on Starling's law was applied to this pump.

The results achieved suffice to validate the main objectives of this work. Concepts of the cardiovascular system were studied to ensure that the modeling of physiological systems and the simulation results are in accordance with the literature.

It is important to emphasize that until the writing of this work, researchers at the Universidade Federal de Alagoas did not have conditions to perform either *in vitro* or *in vivo* studies of LVADs. Because of that, numerical simulations are essential, and the framework developed in this work will give them a more comprehensive vision of the hemodynamical variables than the previous one, which considers only the left side of the heart. This framework is left as a legacy for future research.

Finally, this work will allow plenty of future investigations. For instance, different types of VADs can be coupled to this framework and studied, including right ventricular assist devices (RVADs). Two VADs coupled at the same time, BiVADs, are a great object of study. Additionally, other physiological control techniques can be applied to any VAD coupled to this framework, including more complex implementations of the Starling-like controller, such as the adaptive Starling-like controller, that allows simulation of exercise conditions and it considers different control lines by changing the scaling factor.

Bibliography

- [1] “Cardiovascular diseases (cvds).” [Online]. Available: [https://www.who.int/en/news-room/fact-sheets/detail/cardiovascular-diseases-\(cvds\)](https://www.who.int/en/news-room/fact-sheets/detail/cardiovascular-diseases-(cvds))
- [2] A. C. Guyton, J. E. Hall *et al.*, *Textbook of medical physiology*. Elsevier, 2015.
- [3] G. Sayer, Y. Naka, and U. P. Jorde, “Ventricular assist device therapy,” *Cardiovascular therapeutics*, vol. 27, no. 2, pp. 140–150, 2009.
- [4] A.-H. H. AlOmari, A. V. Savkin, M. Stevens, D. G. Mason, D. L. Timms, R. F. Salomonson, and N. H. Lovell, “Developments in control systems for rotary left ventricular assist devices for heart failure patients: a review,” *Physiological measurement*, vol. 34, no. 1, p. R1, 2012.
- [5] L. F. V. Silva, T. D. Cordeiro, and A. M. N. Lima, “A variable gain physiological controller for a rotary left ventricular assist device,” in *2021 43rd Annual International Conference of the IEEE Engineering in Medicine and Biology Society (EMBC)*, 2021, pp. 5606–5609.
- [6] H. G. de Melo Santos, M. F. F. da Silva Patriota, R. d. A. M. Junior, L. F. V. Silva, T. D. Cordeiro, and A. M. N. Lima, “Investigando a importância do instante de ejeção de dispositivos de assistência ventricular pulsáteis para o desempenho de controladores síncronos,” in *Simpósio Brasileiro de Automação Inteligente-SBAI*, vol. 1, no. 1, 2021.
- [7] T. D. Cordeiro, D. L. Sousa, I. A. Cestari, and A. M. Lima, “A physiological control system for ecg-synchronized pulsatile pediatric ventricular assist devices,” *Biomedical Signal Processing and Control*, vol. 57, p. 101752, 2020.
- [8] M. A. Simaan, A. Ferreira, S. Chen, J. F. Antaki, and D. G. Galati, “A dynamical state space representation and performance analysis of a feedback-controlled rotary left ventricular assist device,” *IEEE Transactions on Control Systems Technology*, vol. 17, no. 1, pp. 15–28, 2008.
- [9] T. D. Cordeiro, “Sistema de controle fisiológico aplicado a dispositivos de assistência ventricular,” Ph.D. dissertation, Universidade Federal de Campina Grande, 2017.

- [10] L. Formaggia and A. Veneziani, “Geometrical multiscale models for the cardiovascular system: from lumped parameters to 3d simulations,” 2003.
- [11] A. Di Molfetta, L. Santini, G. Forleo, M. Cesario, C. Tota, M. Sgueglia, D. Sergi, G. Ferrari, and F. Romeo, “Use of a comprehensive numerical model to improve biventricular pacemaker temporization in patients affected by heart failure undergoing to crt-d therapy,” *Medical & biological engineering & computing*, vol. 48, no. 8, pp. 755–764, 2010.
- [12] G. Ferrari, C. De Lazzari, R. Mimmo, G. Tosti, and D. Ambrosi, “A modular numerical model of the cardiovascular system for studying and training in the field of cardiovascular physiopathology,” *Journal of biomedical engineering*, vol. 14, no. 2, pp. 91–107, 1992.
- [13] H. Suga and K. Sagawa, “Instantaneous pressure-volume relationships and their ratio in the excised, supported canine left ventricle,” *Circulation research*, vol. 35, no. 1, pp. 117–126, 1974.
- [14] T. Korakianitis and Y. Shi, “A concentrated parameter model for the human cardiovascular system including heart valve dynamics and atrioventricular interaction,” *Medical engineering & physics*, vol. 28, no. 7, pp. 613–628, 2006.
- [15] A. Z. Hunsberger, “Modeling and analysis of interactions between a pulsatile pneumatic ventricular assist device and the left ventricle,” Ph.D. dissertation, University of Pittsburgh, 2005.
- [16] N. S. Nise, *Control systems engineering*. John Wiley & Sons, 2020.
- [17] E. J. Molina, P. Shah, M. S. Kiernan, W. K. Cornwell III, H. Copeland, K. Takeda, F. G. Fernandez, V. Badhwar, R. H. Habib, J. P. Jacobs *et al.*, “The society of thoracic surgeons intermacs 2020 annual report,” *The Annals of thoracic surgery*, vol. 111, no. 3, pp. 778–792, 2021.
- [18] D. Timms, “A review of clinical ventricular assist devices,” *Medical engineering & physics*, vol. 33, no. 9, pp. 1041–1047, 2011.
- [19] J. J. Han, M. A. Acker, and P. Atluri, “Left ventricular assist devices: synergistic model between technology and medicine,” *Circulation*, vol. 138, no. 24, pp. 2841–2851, 2018.
- [20] L. E. Rodriguez, E. E. Suarez, M. Loebe, and B. A. Bruckner, “Ventricular assist devices (vad) therapy: new technology, new hope?” *Methodist DeBakey cardiovascular journal*, vol. 9, no. 1, p. 32, 2013.
- [21] S. Choi, J. Boston, D. Thomas, and J. F. Antaki, “Modeling and identification of an axial flow blood pump,” in *Proceedings of the 1997 American Control Conference (Cat. No. 97CH36041)*, vol. 6. IEEE, 1997, pp. 3714–3715.

-
- [22] A. C. Guyton, “Determination of cardiac output by equating venous return curves with cardiac response curves,” *Physiological reviews*, vol. 35, no. 1, pp. 123–129, 1955.
- [23] A. F. Stephens, M. C. Stevens, S. D. Gregory, M. Kleinheyder, and R. F. Salamonsen, “In vitro evaluation of an immediate response starling-like controller for dual rotary blood pumps,” *Artificial Organs*, vol. 41, no. 10, pp. 911–922, 2017.
- [24] A. Stephens, S. Gregory, G. Tansley, A. Busch, and R. Salamonsen, “In vitro evaluation of an adaptive starling-like controller for dual rotary ventricular assist devices,” *Artificial Organs*, vol. 43, no. 11, pp. E294–E307, 2019.